

Combining Planck and SPT cluster catalogs: cosmological analysis and impact on Planck scaling relation calibration*

L. SALVATI,^{1,2,3} A. SARO,^{4,1,2,5} S. BOCQUET,⁶ M. COSTANZI,^{1,2,4} B. ANSARINEJAD,⁷ B. A. BENSON,^{8,9,10} L. E. BLEEM,^{11,12} M. S. CALZADILLA,¹³ J. E. CARLSTROM,^{9,10,14,15,16} C. L. CHANG,^{15,9,10} R. CHOWN,¹⁷ A. T. CRITES,^{18,9,10} T. DE HAAN,^{19,20} M. A. DOBBS,^{21,22} W. B. EVERETT,²³ B. FLOYD,²⁴ S. GRANDIS,²⁵ E. M. GEORGE,^{26,20} N. W. HALVERSON,^{23,27} G. P. HOLDER,^{28,29} W. L. HOLZAPFEL,²⁰ J. D. HRUBES,³⁰ A. T. LEE,^{20,31} D. LUONG-VAN,³⁰ M. McDONALD,³² J. J. MCMAHON,^{9,10,14,16} S. S. MEYER,^{9,10,14,16} M. MILLEA,²⁰ L. M. MOCANU,^{9,10} J. J. MOHR,^{33,34,35} T. NATOLI,^{9,10} Y. OMORI,^{9,10,36,37} S. PADIN,^{38,9,10} C. PRYKE,³⁹ C. L. REICHARDT,⁷ J. E. RUHL,⁴⁰ F. RUPPIN,^{41,42} K. K. SCHAFFER,^{43,9,16} T. SCHRABBACK,⁴⁴ E. SHIROKOFF,^{9,10,20} Z. STANISZEWSKI,^{45,40} A. A. STARK,⁴⁶ J. D. VIEIRA,^{28,29} AND R. WILLIAMSON^{45,9,10}

¹INAF – Osservatorio Astronomico di Trieste, Via G. B. Tiepolo 11, 34143 Trieste, Italy

²IFPU – Institute for Fundamental Physics of the Universe, Via Beirut 2, 34014 Trieste, Italy

³Université Paris-Saclay, CNRS, Institut d’Astrophysique Spatiale, 91405, Orsay, France

⁴Dipartimento di Fisica, Sezione di Astronomia, Università di Trieste, Via Tiepolo 11, I-34143 Trieste, Italy

⁵INFN – Sezione di Trieste, I-34100 Trieste, Italy

⁶Max-Planck-Institut für Astrophysik (MPA), Karl-Schwarzschild Strasse 1, 85748 Garching bei München, Germany

⁷School of Physics, University of Melbourne, Parkville, VIC 3010, Australia

⁸Fermi National Accelerator Laboratory, MS209, P.O. Box 500, Batavia, IL 60510

⁹Kavli Institute for Cosmological Physics, University of Chicago, Chicago, IL, USA 60637

¹⁰Department of Astronomy and Astrophysics, University of Chicago, Chicago, IL, USA 60637

¹¹High Energy Physics Division, Argonne National Laboratory, 9700 South Cass Avenue, Lemont, IL 60439, USA

¹²Kavli Institute for Cosmological Physics, University of Chicago, 5640 South Ellis Avenue, Chicago, IL 60637, USA

¹³Kavli Institute for Astrophysics and Space Research, Massachusetts Institute of Technology Cambridge, MA 02139, USA

¹⁴Department of Physics, University of Chicago, Chicago, IL, USA 60637

¹⁵High Energy Physics Division, Argonne National Laboratory, Argonne, IL, USA 60439

¹⁶Enrico Fermi Institute, University of Chicago, Chicago, IL, USA 60637

¹⁷Department of Physics and Astronomy, McMaster University, 1280 Main St. W., Hamilton, ON L8S 4L8, Canada

¹⁸Department of Astronomy & Astrophysics, University of Toronto, 50 St George St, Toronto, ON, M5S 3H4, Canada

¹⁹High Energy Accelerator Research Organization (KEK), Tsukuba, Ibaraki 305-0801, Japan

²⁰Department of Physics, University of California, Berkeley, CA, USA 94720

²¹Department of Physics and McGill Space Institute, McGill University, Montreal, Quebec H3A 2T8, Canada

²²Canadian Institute for Advanced Research, CIFAR Program in Cosmology and Gravity, Toronto, ON, M5G 1Z8, Canada

²³Center for Astrophysics and Space Astronomy, Department of Astrophysical and Planetary Sciences, University of Colorado, Boulder, CO, 80309

²⁴Department of Physics and Astronomy, University of Missouri–Kansas City, 5110 Rockhill Road, Kansas City, MO 64110, USA

²⁵Faculty of Physics, Ludwig-Maximilians-Universität, Scheinerstr. 1, 81679, Munich, Germany

²⁶European Southern Observatory, Karl-Schwarzschild-Straße 2, 85748 Garching, Germany

²⁷Department of Physics, University of Colorado, Boulder, CO, 80309

²⁸Astronomy Department, University of Illinois at Urbana-Champaign, 1002 W. Green Street, Urbana, IL 61801, USA

²⁹Department of Physics, University of Illinois Urbana-Champaign, 1110 W. Green Street, Urbana, IL 61801, USA

³⁰University of Chicago, Chicago, IL, USA 60637

³¹Physics Division, Lawrence Berkeley National Laboratory, Berkeley, CA, USA 94720

³²Kavli Institute for Astrophysics and Space Research, Massachusetts Institute of Technology, 77 Massachusetts Avenue, Cambridge, MA 02139

³³Faculty of Physics, Ludwig-Maximilians-Universität, 81679 München, Germany

³⁴Excellence Cluster ORIGINS, Boltzmannstr. 2, 85748 Garching, Germany

³⁵Max-Planck-Institut für extraterrestrische Physik, 85748 Garching, Germany

³⁶Kavli Institute for Particle Astrophysics and Cosmology, Stanford University, 452 Lomita Mall, Stanford, CA 94305

Corresponding author: Laura Salvati
laura.salvati@inaf.it,
laura.salvati@universite-paris-saclay.fr

* Released on ...

³⁷Dept. of Physics, Stanford University, 382 Via Pueblo Mall, Stanford, CA 94305

³⁸California Institute of Technology, Pasadena, CA, USA 91125

³⁹Department of Physics, University of Minnesota, Minneapolis, MN, USA 55455

⁴⁰Physics Department, Center for Education and Research in Cosmology and Astrophysics, Case Western Reserve University, Cleveland, OH, USA 44106

⁴¹Univ. Lyon, Univ. Claude Bernard Lyon 1, CNRS/IN2P3, IP2I Lyon, F-69622, Villeurbanne, France

⁴²Kavli Institute for Astrophysics & Space Research, Massachusetts Institute of Technology, 77 Massachusetts Ave., Cambridge, MA 02139, USA

⁴³Liberal Arts Department, School of the Art Institute of Chicago, Chicago, IL, USA 60603

⁴⁴Argelander Institut für Astronomie, Auf dem Hügel 71, D-53121 Bonn, Germany

⁴⁵Jet Propulsion Laboratory, California Institute of Technology, Pasadena, CA 91109, USA

⁴⁶Center for Astrophysics | Harvard & Smithsonian, 60 Garden Street, Cambridge, MA 02138, USA

Submitted to APJ

ABSTRACT

We provide the first combined cosmological analysis of South Pole Telescope (SPT) and Planck cluster catalogs. The aim is to provide an independent calibration for Planck scaling relations, exploiting the cosmological constraining power of the SPT-SZ cluster catalog and its dedicated weak lensing (WL) and X-ray follow-up observations. We build a new version of the Planck cluster likelihood. In the $\nu\Lambda$ CDM scenario, focusing on the mass slope and mass bias of Planck scaling relations, we find $\alpha_{\text{SZ}} = 1.49_{-0.10}^{+0.07}$ and $(1-b)_{\text{SZ}} = 0.69_{-0.14}^{+0.07}$ respectively. The results for the mass slope show a $\sim 4\sigma$ departure from the self-similar evolution, $\alpha_{\text{SZ}} \sim 1.8$. This shift is mainly driven by the matter density value preferred by SPT data, $\Omega_m = 0.30 \pm 0.03$, lower than the one obtained by Planck data alone, $\Omega_m = 0.37_{-0.06}^{+0.02}$. The mass bias constraints are consistent both with outcomes of hydrodynamical simulations and external WL calibrations, $(1-b) \sim 0.8$, and with results required by the Planck cosmic microwave background cosmology, $(1-b) \sim 0.6$. From this analysis, we obtain a new catalog of Planck cluster masses M_{500} . We estimate the relation between the published Planck derived M_{SZ} masses and our derived masses, as a measured mass bias. We analyse the mass, redshift and detection noise dependence of this quantity, finding an increasing trend towards high redshift and low mass. These results mimic the effect of departure from self-similarity in cluster evolution, showing different dependencies for the low-mass high-mass, low- z high- z regimes.

Keywords: cosmological parameters – cosmology: observations – galaxies: clusters: general – large-scale structure of universe

1. INTRODUCTION

Galaxy clusters are the largest, gravitationally bound structures in the Universe. These objects represent the nodes in the cosmic web of the large scale structure, and are related to the peaks in the density field, on scales of the order of megaparsec.

Galaxy clusters can be detected in different wavelengths. In recent years, several experiments produced large catalogs of clusters to be used for the cosmological analysis, such as the Planck survey (Planck Collaboration et al. 2016a,b), the South Pole Telescope (SPT hereafter) (Bleem et al. 2015; de Haan et al. 2016; Bocquet et al. 2019) and the Atacama Cosmology Telescope (Hilton et al. 2021) in the millimeter wavelengths; the Kilo-Degree Survey (Maturi et al. 2019), the Dark Energy Survey (Drlica-Wagner et al. 2018; Abbott et al.

2020) in optical; the ROSAT survey (Böhringer et al. 2017), the XXL survey (Adami et al. 2018; Pacaud et al. 2018) and the first eROSITA observations (Liu et al. 2021) in X-rays. In particular, the abundance of galaxy clusters (galaxy cluster number counts) has emerged as a fundamental cosmological probe. Cluster formation and evolution is strictly related to the underlying cosmological model, tracing the growth of structures, see e.g. Allen et al. (2011). The cosmological analysis of clusters provides constraints on the total matter density Ω_m and on the σ_8 parameter, which is the rms fluctuation in the linear matter density field on 8 Mpc/ h scale at redshift $z = 0$. Comparing and combining these results with other cosmological probes, such as cosmic microwave background radiation (CMB hereafter) at high redshift, or baryon acoustic oscillations (BAO hereafter)

at low redshift, allows us to perform fundamental consistency checks of the standard cosmological model.

The cosmological analysis of galaxy clusters is based on the knowledge of their mass and redshift distribution, which is described, theoretically, through the halo mass function, see e.g. discussion in Monaco (2016) and references therein for an updated list of available mass function evaluations, and McClintock et al. (2019); Bocquet et al. (2020) for recent mass function emulators. However, cluster mass cannot be measured directly. Observations focus therefore on mass-proxies, that show a tight correlation with the cluster mass. Cluster masses and survey observables are linked through statistical scaling relations, that describe the interplay between astrophysics and cosmology in the cluster formation and evolution. The scaling relation calibration represents the largest source of systematic uncertainty in current cluster cosmology studies.

Scaling relations are combined with a model for the selection process (i.e. a selection function) to transform the theoretical halo mass function into a prediction for the distribution of clusters in the space of redshift and survey observables. In this scenario, it is clear that a precise and comprehensive characterisation of the mass function, the scaling relations and the selection function is needed in order to provide stringent and unbiased constraints on cosmological parameters from galaxy clusters.

In this work, we perform the first combined cosmological analysis of the SPT (Bleem et al. 2015) and Planck (Planck Collaboration et al. 2016a) cluster catalogs. Both experiments detect clusters in the millimeter wavelengths, through the thermal Sunyaev-Zeldovich (tSZ hereafter) effect (Sunyaev & Zeldovich 1970). The strength of this analysis lies in the combination of a full-sky survey (Planck) with deep and high-resolution observations from a ground-based experiment (SPT). The combination of the two cluster catalogs spans a large redshift range (from $z = 0$ for Planck catalog, up to $z \sim 1.7$ for the SPT one), ensuring the possibility to test the impact of astrophysical processes on the cosmological evolution of clusters. The strength of combining Planck and SPT cluster observations has been already explored in the analysis of Melin et al. (2021), in which the authors provide a new cluster catalog extracted from the common area observed by the two experiments.

Our analysis is the first in a series of papers in which we exploit the combination of the SPT-SZ and Planck cluster catalogs. In this work, we focus on the calibration of Planck scaling relations, i.e. the mass-calibration problem. As mentioned before, cluster masses cannot be measured directly. With tSZ observations, we can

obtain a mass evaluation, M_{SZ} , from the cluster pressure profile, assuming hydrostatic equilibrium (HE hereafter), see e.g. Pratt et al. (2019). Nevertheless, from numerical simulations we expect the HE assumption to provide biased-low masses, by a factor of $\sim 20\%$, see Pratt et al. (2019) and reference therein. In order to take into account this difference, we introduce a mass bias parameter in the analysis, defined through the ratio between M_{SZ} and the real cluster mass. In the original Planck analysis, the baseline calibration of the mass bias and the entire scaling relations is based on the use of external X-ray and weak lensing (WL hereafter) measurements, see Planck Collaboration et al. (2016b).

It has been shown that mass calibration played an important role in the CMB-cluster σ_8 tension (Planck Collaboration et al. 2014, 2016b). Recent analyses of Planck data (Aghanim et al. 2016; Salvati et al. 2018; Planck Collaboration et al. 2020a) reveal that cosmological results are now consistent between CMB primary anisotropies and galaxy clusters. In particular, constraints on the σ_8 parameter are now well in agreement within 2σ . Nevertheless, different choices for the mass bias calibration (and the scaling relation calibration in general) largely affect the cosmological constraints, in particular shifting the σ_8 results, see e.g. Planck Collaboration et al. (2016b).

Therefore, with this analysis, we aim to provide an independent calibration for Planck scaling relations, exploiting the cosmological constraining power of the SPT-SZ cluster catalog and the X-ray and WL follow-up data used for direct mass calibration (Bocquet et al. 2019; McDonald et al. 2013, 2017; Dietrich et al. 2019; Schrabback et al. 2018).

The paper is structured as follows: in section 2 we describe the cluster observations for Planck and SPT and the underlying theoretical model for the use of cluster number counts. In section 3 we discuss the approach used to combine the datasets and extract cosmological information. We present and discuss the results in sections 4 and 5, and derive our final conclusions in section 6.

2. DATA AND MODEL

In this section we summarise the observation and detection strategies for the Planck and SPT experiments. We also describe the theoretical models that lead to the evaluation of the likelihood function needed for the cosmological analysis. For the full discussion, we refer to the SPT analysis in Bleem et al. (2015); Bocquet et al. (2019) and the Planck analysis in Planck Collaboration et al. (2016b,a).

We recall here that clusters detected through the tSZ effect are often defined as objects with a mass M_{500} contained in a sphere of radius R_{500} , such that the cluster mean mass overdensity inside R_{500} corresponds to 500 times the critical density $\rho_c(z)$. Therefore we define the total cluster mass as

$$M_{500} = \frac{4\pi}{3} R_{500}^3 500 \rho_c(z). \quad (1)$$

2.1. South Pole Telescope

The South Pole Telescope is a 10m diameter telescope located at the geographic South Pole (Carlstrom et al. 2011). We consider observations of the SPT-SZ survey, which detected galaxy clusters through the tSZ effect, using observations in the 95 and 150 GHz bands, in a 2500 deg² area. With $\sim 1'$ resolution and 1° field of view, SPT is able to observe rare, high-mass clusters, from redshift $z \gtrsim 0.2$.

Galaxy clusters are extracted from the SPT-SZ survey data through a multi-matched filter technique, see e.g. Melin et al. (2006). This approach makes use of the known (non-relativistic) tSZ spectral signature and a model for the spatial profile of the signal. In the standard SPT analysis approach, the spatial profile follows the projected isothermal β model (Cavaliere & Fusco-Femiano 1976), with β fixed to 1.

The tSZ signature is then used, together with a description of the noise sources in the frequency maps, to construct a filter designed to maximize the sensitivity to galaxy clusters. From the filtered maps, we can extract cluster candidates, via a peak detection algorithm similar to the SExtractor routine (Bertin & Arnouts 1996). In SPT analysis, the maximum detection significance ξ is used as tSZ observable. We also make use of the unbiased tSZ significance ζ , defined as

$$\langle \xi \rangle^2 = \zeta^2 + 3. \quad (2)$$

In this work we focus on the cosmological cluster sample, analyzed in de Haan et al. (2016); Bocquet et al. (2019). It is a subsample of the full SPT-SZ sample (Bleem et al. 2015), consisting of 365 detections (343 of which have been optically confirmed), restricted to $z > 0.25$ and with a detection significance $\xi > 5$.

Following the analysis in Bocquet et al. (2019), we make use of a multi-wavelength approach, considering also WL and X-ray data. In detail, we use WL measurements of 32 clusters, considering the reduced tangential shear profiles in angular coordinates (corrected for contamination by cluster galaxies) and the estimated redshift distributions of the selected source galaxies. These measurements are obtained with Magellan/Megacam (Dietrich et al. 2019) for 19 clusters in the redshift range

$0.29 \leq z \leq 0.69$, and with the Advanced Camera for Surveys on board of the Hubble Space Telescope (HST hereafter) (Schrabback et al. 2018) for 13 clusters in the redshift range $0.576 \leq z \leq 1.132$.

For the X-ray measurements, we consider a sample of 89 clusters up to high redshift observed by Chandra (McDonald et al. 2013, 2017). We refer the reader to these works for a detailed discussion on the X-ray observation and analysis techniques. The observables that we use in this analysis are the total gas mass M_{gas} within an outer radius ranging from 80 to 2000 kpc, and the spectroscopic temperature T_X in the $0.15R_{500} - R_{500}$ range.

The SPT cluster cosmological analysis is based on a multi-observable Poissonian likelihood. We report here the fundamental steps and refer the reader to the full discussion in Bocquet et al. (2019). The SPT likelihood function can be written as

$$\begin{aligned} \ln \mathcal{L}_{\text{SPT}} = & \sum_i \ln \frac{dN(\xi, z|\mathbf{p})}{d\xi dz} \Big|_{\xi_i, z_i} \\ & - \int_{z_{\text{cut}}}^{\infty} dz \int_{\xi_{\text{cut}}}^{\infty} d\xi \frac{dN(\xi, z|\mathbf{p})}{d\xi dz} \\ & + \sum_j \ln P(Y_X, g_t | \xi_j, z_j, \mathbf{p}) \Big|_{Y_{X_j}, g_{t_j}}. \end{aligned} \quad (3)$$

In the above equation, \mathbf{p} is the vector of cosmological and scaling relation parameters, the first sum is over all the i clusters in the cosmological sample, while the second sum is for the j clusters with the Y_x and/or WL measurements, with g_t being the reduced tangential shear profile. Therefore, the first two terms represent the tSZ cluster abundance, while the third represents the information from follow-up mass calibration.

We can now explicitly evaluate the different terms in Eq. 3. The first term is given by

$$\begin{aligned} \frac{dN(\xi, z|\mathbf{p})}{d\xi dz} = & \iint dM_{500} d\zeta [P(\xi|\zeta)P(\zeta|M_{500}, z, \mathbf{p}) \\ & \times \frac{dN(M_{500}, z|\mathbf{p})}{dM_{500}} \Omega(z, \mathbf{p})]. \end{aligned} \quad (4)$$

In the above equation, $\Omega(z, \mathbf{p})$ is the survey volume, $dN(M_{500}, z|\mathbf{p})/dM_{500}$ is the halo mass function, $P(\zeta|M_{500}, z, \mathbf{p})$ is the intrinsic scatter and $P(\xi|\zeta)$ is the measurement uncertainty. Therefore, the first term in Eq. 3 is obtained evaluating Eq. 4 at the measured (ξ_i, z_i) for each cluster, marginalizing over photometric redshift errors where present. The second term is simply evaluated through a two-dimensional integral over Eq. 4.

The last term in Eq. 3 represents the mass calibration contribution and can be evaluated as

$$\begin{aligned}
& P(Y_X^{\text{obs}}, g_t^{\text{obs}} | \xi, z, \mathbf{p}) \\
&= \iiint dM_{500} d\zeta dY_X dM_{\text{WL}} \\
&\times [P(Y_X^{\text{obs}} | Y_X) P(g_t^{\text{obs}} | M_{\text{WL}}) P(\xi | \zeta) \\
&\times P(\zeta, Y_X, M_{\text{WL}} | M_{500}, z, \mathbf{p}) P(M_{500} | z, \mathbf{p})] . \quad (5)
\end{aligned}$$

In the above equation $P(M_{500} | z, \mathbf{p})$ is the normalized halo mass function and the multi-observable scaling relation $P(\zeta, Y_X, M_{\text{WL}} | M_{500}, z, \mathbf{p})$ takes into account the effect of correlated scatter. For the detailed discussion on how to evaluate this multidimensional integral, we refer again the reader to [Bocquet et al. \(2019\)](#).

The SPT cosmological sample contains 22 tSZ detections with unknown redshift, since they have not been confirmed through optical counterparts. As detailed in [Bocquet et al. \(2019\)](#), this number is consistent with the expected number of false detections above $\xi = 5$. Therefore, discarding these objects does not affect the cosmological results.

Following [Bocquet et al. \(2019\)](#), we consider three different proxies for the cluster mass: the unbiased tSZ significance ζ , defined in Eq. 2, the X-ray Y_X quantity and the WL mass M_{WL} . The corresponding mean observable-mass scaling relations are defined as

$$\begin{aligned}
\langle \ln \zeta \rangle &= \ln A_{\text{SZ}} + B_{\text{SZ}} \left(\frac{M_{500} h_{70}}{4.3 \times 10^{14} M_{\odot}} \right) \\
&+ C_{\text{SZ}} \ln \left(\frac{E(z)}{E(0.6)} \right) \quad (6)
\end{aligned}$$

$$\begin{aligned}
\ln \left(\frac{M_{500} h_{70}}{8.37 \times 10^{13} M_{\odot}} \right) &= \ln A_{Y_X} + B_{Y_X} \langle \ln Y_X \rangle \\
&+ B_{Y_x} \ln \left(\frac{h_{70}^{5/2}}{3 \times 10^{14} M_{\odot} \text{keV}} \right) \\
&+ C_{Y_X} \ln E(z) \quad (7)
\end{aligned}$$

$$\langle \ln M_{\text{WL}} \rangle = \ln b_{\text{WL}} + \ln M_{500} . \quad (8)$$

The intrinsic scatter for $\ln \zeta$, $\ln Y_X$ and $\ln M_{\text{WL}}$ is described by normal distributions, characterized by $\sigma_{\ln \zeta}$, $\sigma_{\ln Y_X}$ and σ_{WL} respectively. These widths are assumed to be constant with respect to mass and redshift. The full description of the WL bias, b_{WL} , and the associated scatter is done in [Bocquet et al. \(2019\)](#), we only recall here that the modelling introduces six nuisance parameters δ_i , reported in Table 1. We also take into account possible scatter correlations between the three mass proxies, defining the correlation parameters $\rho_{\text{SZ-X}}$, $\rho_{\text{SZ-WL}}$ and $\rho_{\text{X-WL}}$. All the parameters characterizing the scaling relations are listed and defined in Table 1.

2.2. Planck satellite

The Planck satellite is a mission from the European Space Agency (ESA), which concluded the observations in 2013 ([Planck Collaboration et al. 2020b](#)). The Planck cluster catalog ([Planck Collaboration et al. 2016a](#)) is based on full-sky observations from the 6 channels of the High Frequency Instrument (HFI, [Planck Collaboration et al. \(2020c\)](#)), in the frequency range 100-857 GHz. Similarly to SPT, Planck clusters are extracted using a multi-frequency matched filter technique. For the spatial profile of the signal, the so-called ‘‘universal pressure profile’’ from [Arnaud et al. \(2010\)](#) has been adopted.

The cosmological sample, labeled as ‘‘PSZ2 cosmo’’, consists of 439 clusters, 433 of which have confirmed redshifts, detected with a signal-to-noise ratio $q > 6$, on the 65% of the sky remaining after masking high dust emission regions and point sources. The signal-to-noise ratio is defined as

$$q = \frac{Y_{500}}{\sigma_f(\theta_{500}, l, b)} , \quad (9)$$

where Y_{500} is the integrated compton parameter (tSZ signal for a cluster) and $\sigma_f(\theta_{500}, l, b)$ is the detection filter noise (given the cluster angular size, θ_{500} , and sky position in galactic coordinates (l, b)). The PSZ2-cosmo sample spans the mass range $M_{\text{SZ}} = (2 - 10) \times 10^{14} M_{\odot}$ and the redshift range $z = [0, 1]$.

The Planck cosmological analysis is based on a Poissonian likelihood, constructed on counts of redshift and signal-to-noise ratio:

$$\ln \mathcal{L}_{\text{P}} = \sum_{i,j}^{N_z N_q} [N_{ij} \ln \bar{N}_{ij} - \bar{N}_{ij} - \ln(N_{ij}!)] . \quad (10)$$

In the above equation, N_z and N_q are the total number of redshift and signal-to-noise bins, with redshift binning $\Delta z = 0.1$ and signal-to-noise ratio binning $\Delta \log q = 0.25$. N_{ij} represents the observed number counts of cluster. \bar{N}_{ij} is the predicted mean number of objects in each bin, modelled by theory as

$$\bar{N}_{ij} = \frac{dN}{dzdq}(z_i, q_j) \Delta z \Delta q . \quad (11)$$

We report here the main steps to evaluate the theoretical cluster number counts and refer to [Planck Collaboration et al. \(2016b\)](#) for the complete description. The cluster distribution can be written as

$$\frac{dN}{dzdq} = \iint d\Omega dM_{500} \frac{dN}{dzdM_{500}d\Omega} P[q | \bar{q}_m(M_{500}, z, l, b)] , \quad (12)$$

Table 1. Cosmological and scaling relation parameters, following the definitions in [Bocquet et al. \(2019\)](#) and [Planck Collaboration et al. \(2016b\)](#). We report a brief description and the prior we adopt in our analysis: a range indicates a top-hat prior, while $\mathcal{N}(\mu, \sigma)$ stands for a Gaussian prior with mean μ and variance σ^2 .

Parameter	Description	Prior
Cosmology		
Ω_m	Matter density	[0.15, 0.4]
A_s	Amplitude of primordial curvature perturbations	$[10^{-10}, 10^{-8}]$
h	Expansion rate	[0.55, 0.9]
$\Omega_b h^2$	Baryon density	[0.020, 0.024]
$\Omega_\nu h^2$	Massive neutrinos energy density	[0.0006, 0.01]
n_s	Spectral index	[0.94, 1.0]
SPT: SZ scaling relation		
A_{SZ}	Amplitude	[1, 10]
B_{SZ}	Power-law index mass dependence	[1.2, 2]
C_{SZ}	Power-law index redshift evolution	[-1, 2]
$\sigma_{\ln \zeta}$	Intrinsic scatter	[0.01, 0.5]
SPT: X-ray Y_X scaling relation		
A_{Y_X}	Amplitude	[3, 10]
B_{Y_X}	Power-law index mass dependence	[0.3, 0.9]
C_{Y_X}	Power-law index redshift evolution	[-1, 5]
$\sigma_{\ln Y_X}$	Intrinsic scatter	[0.01, 0.5]
$d \ln Y_X / d \ln r$	Radial slope Y_X profile	$\mathcal{N}(1.12, 0.23)$
SPT: M_{WL} scaling relation		
$\delta_{WL, \text{bias}}$	Coeff. for WL bias	$\mathcal{N}(0, 1)$
δ_{Megacam}	Coeff. for error on WL bias	$\mathcal{N}(0, 1)$
δ_{HST}	Coeff. for error on WL bias	$\mathcal{N}(0, 1)$
$\delta_{WL, \text{scatter}}$	Coeff. for lognormal scatter	$\mathcal{N}(0, 1)$
$\delta_{WL, \text{LSS}_{\text{Megacam}}}$	Coeff. for normal scatter	$\mathcal{N}(0, 1)$
$\delta_{WL, \text{LSS}_{\text{HST}}}$	Coeff. for normal scatter	$\mathcal{N}(0, 1)$
SPT: Correlation coefficients between scatters		
$\rho(\text{SZ}, \text{WL})$	Correlation coefficient SZ-WL	[-1, 1]
$\rho(\text{SZ}, \text{X})$	Correlation coefficient SZ-X	[-1, 1]
$\rho(\text{X}, \text{WL})$	Correlation coefficient X-WL	[-1, 1]
Planck: SZ scaling relation		
α_{SZ}	Power-law index mass dependence	[1, 2.5]
β_{SZ}	Power-law index redshift dependence	Fixed(0.66) or [0, 2]
$\sigma_{\log Y_{SZ}}$	Intrinsic scatter	$\mathcal{N}(0.075, 0.01)$
$\log Y_{*SZ}$	Amplitude	$\mathcal{N}(-0.186, 0.021)$
$(1 - b)_{SZ}$	Mass bias	[0.3, 1.3]

where

$$\frac{dN}{dz dM_{500} d\Omega} = \frac{dV}{dz d\Omega} \frac{dN}{dV dM_{500}} \quad (13)$$

is the product of the volume element and the halo mass function respectively.

In Eq. 12, the quantity $P[q|\bar{q}_m(M_{500}, z, l, b)]$ represents the distribution of the signal-to-noise ratio q given the mean value $\bar{q}_m(M_{500}, z, l, b)$, predicted by the model, for a cluster located at position (l, b) , with mass M_{500}

and redshift z . The $P[q|\bar{q}_m]$ distribution takes into account the noise fluctuations and the intrinsic scatter $\sigma_{\ln Y}$ of the actual cluster signal Y_{500} around the mean value, $\bar{Y}_{500}(M_{500}, z)$, predicted from the scaling relation. In this analysis, we assume that the intrinsic scatter does not show any dependence on (M_{500}, z) , following the original approach in [Planck Collaboration et al. \(2016b\)](#).

The relation between the cluster observables Y_{500} , θ_{500} and the cluster mass and redshift is described by a log-

normal distribution function $P(\ln Y_{500}, \theta_{500} | M_{500}, z)$. The mean values of this distribution are given by the scaling relations $\bar{Y}_{500}(M_{500}, z)$ and $\bar{\theta}_{500}(M_{500}, z)$, defined as

$$E^{-\beta_{\text{SZ}}}(z) \left[\frac{D_A^2(z) \bar{Y}_{500}}{10^{-4} \text{Mpc}^2} \right] = Y_{*,\text{SZ}} \left[\frac{h}{0.7} \right]^{-2+\alpha_{\text{SZ}}} \times \left[\frac{(1-b)_{\text{SZ}} M_{500}}{6 \times 10^{14} M_{\odot}} \right]^{\alpha_{\text{SZ}}} \quad (14)$$

$$\bar{\theta}_{500} = \theta_* \left[\frac{h}{0.7} \right]^{-2/3} \left[\frac{(1-b)_{\text{SZ}} M_{500}}{6 \times 10^{14} M_{\odot}} \right]^{1/3} \times E^{-2/3}(z) \left[\frac{D_A(z)}{500 \text{Mpc}} \right]^{-1}. \quad (15)$$

In the above equations, $D_A(z)$ is the angular diameter distance and $E(z) \equiv H(z)/H_0$.

The calibration of Eqs. 14 and 15 is obtained through a multi-wavelength analysis and provides constraints on the parameters α_{SZ} , $Y_{*,\text{SZ}}$, $(1-b)_{\text{SZ}}$ and β_{SZ} . The list of scaling relation parameters is reported also in Table 1. As discussed in Planck Collaboration et al. (2014, 2016a), following the analysis in Arnaud et al. (2010), the calibration is based on X-ray observations of 71 clusters and the evaluation of the cluster mass M_{SZ} is obtained through the HE assumption for the intracluster gas. To account for possible deviations from this assumption (due to cluster physics, observational effects or selection effects), the mass bias parameter b is introduced in the analysis, such that the relation between the real cluster mass and HE one is $M_{\text{SZ}} = (1-b)M_{500}$.

In order to evaluate the mass bias (and therefore the real cluster mass), WL mass determinations are introduced in the analysis. For the baseline cosmological analysis, Planck collaboration adopts the evaluation from the Canadian Cluster Comparison Project (Hoekstra et al. (2015), CCCP hereafter), $(1-b)_{\text{SZ}} = 0.780 \pm 0.092$, based on 20 clusters. We stress that the mass bias is considered as a constant quantity, i.e. not allowing for dependence on the cluster mass and redshift. The baseline values for the scaling relation parameters (from X-ray and WL calibration) are reported in Table 2, following Planck Collaboration et al. (2016b). We note that as baseline we assume the self-similarity model for the redshift evolution of the cluster population. This translates into fixing the β parameter to $\beta_{\text{SZ}} = 2/3$.

In summary, the main difference between Planck and SPT mass calibrations lies in the use of external data (from other cluster samples) for Planck vs. the use of internal data (direct follow-up observations) for SPT.

Table 2. Original calibration of Planck scaling relation parameters. $\mathcal{N}(\mu, \sigma)$ stands for a Gaussian prior with mean μ and variance σ^2 .

Parameter	Value	Parameter	Value
$\log Y_{*,\text{SZ}}$	$\mathcal{N}(-0.19, 0.02)$	$\sigma_{\ln Y_{\text{SZ}}}^a$	$\mathcal{N}(0.173, 0.023)$
α_{SZ}	$\mathcal{N}(1.79, 0.08)$	$(1-b)_{\text{SZ}}$	$\mathcal{N}(0.780, 0.092)$
β_{SZ}	0.66		

NOTE—^a In practice, in the analysis we use the parameter $\sigma_{\log Y_{\text{SZ}}} = \mathcal{N}(0.075, 0.01)$.

Therefore, when analysing Planck data, it is possible to relax some of the external calibration results and provide independent constraints on some of the scaling relation parameters.

3. METHOD

In this section we describe the recipe we follow to combine Planck and SPT data. In particular, we discuss how we modify the original Planck likelihood, in order to provide a proper combination with the SPT one. We describe also the approach we use to provide a new evaluation of Planck cluster masses.

3.1. Combining Planck and SPT cluster likelihoods

In order to combine Planck and SPT cluster likelihoods, it is necessary to take into account the overlapping area of the observed sky and the clusters in common between the two catalogs. We choose to modify the Planck likelihood. In particular, we perform a split in redshift of the entire likelihood. For $z \leq 0.25$, where we do not have cluster data from the SPT-SZ survey, we rely on the original version for the Planck likelihood. For $z > 0.25$, we modify the Planck likelihood, removing the part of the sky observed also by the SPT-SZ survey, and the clusters in common with the SPT-SZ catalog. Hereafter, we refer to this new Planck redshift-split likelihood as ‘‘PvSPLIT’’.

We now discuss in details the approach used to build the $z > 0.25$ part of the likelihood. After applying the galactic and point source mask, the Planck observed sky is made up of 417 patches of $10^\circ \times 10^\circ$ area. We identify 16 patches that fully overlap with the SPT observed sky. We remove those patches from the sky area in the likelihood. Furthermore, we identify 35 patches with a partial overlapping between Planck and SPT sky. In this case, we decide to keep them in the analysis, but reduce the sky fraction in each patch, according to the area that is actually observed by both experiments. The remaining observed sky is shown in Fig. 1, upper panel.

We show in grey the removed patches, due to Planck galactic mask and the Planck-SPT fully overlapped area. In yellow, we highlight the patches that partly overlaps between Planck and SPT-SZ survey.

For the cluster catalog, we remove 27 clusters in common with the SPT-SZ cosmological catalog and 2 clusters that fall in the removed patches. We also introduce redshifts for the 6 clusters whose redshifts was unknown in the original PSZ2-cosmo sample. We report the new redshifts in Table 3, specifying if these values have been obtained from photometric (P) or spectroscopic (S) observations. We show the new cluster distribution in Fig. 1: in the upper panel we show how Planck clusters are distributed on the observed sky, in the lower panel we show the mass-redshift cluster distribution.

Following Eq. 10, the new Planck PvSPLIT likelihood therefore reads

$$\begin{aligned} \ln \mathcal{L}_P &= \ln \mathcal{L}_{P1} + \ln \mathcal{L}_{P2} \\ &= \sum_{i_1, j}^{N_{z_1} N_q} [N_{i_1 j} \ln \bar{N}_{i_1 j} - \bar{N}_{i_1 j} - \ln(N_{i_1 j}!)] \\ &+ \sum_{i_2, j}^{N_{z_2} N_q} [N_{i_2 j} \ln \bar{N}_{i_2 j} - \bar{N}_{i_2 j} - \ln(N_{i_2 j}!)] \quad (16) \end{aligned}$$

where we adopt a binning in redshift of $\Delta z = 0.05$, such that $N_{z_1} = 5$, up to $z \leq 0.25$, and $N_{z_2} = 15$. For the binning in the signal-to-noise ratio, we follow the original analysis, with $\Delta \log q = 0.25$. The total likelihood for the combined analysis of Planck and SPT, following Eqs. 3 and 16, is therefore defined as

$$\ln \mathcal{L}_{\text{TOT}} = \ln \mathcal{L}_{\text{SPT}} + \ln \mathcal{L}_{P1} + \ln \mathcal{L}_{P2}. \quad (17)$$

3.2. Sampling recipe

For the cosmological analysis, we make use of the complete SPT likelihood, described in section 2.1. In particular, we rely on the combination of the SPT-selected clusters with their detection significances and redshifts, together with the WL and X-ray follow-up data, where available. Following the definition in Bocquet et al. (2019), we refer to this data set as ‘‘SPTcl’’ (SPT-SZ + WL + Y_X).

For the Planck part of the likelihood, we use the PvSPLIT version described in the previous section. We adopt the parametrisation for the scaling relations described in Eqs. 14 and 15.

In this analysis, we want to test the capability of the Planck+SPT combination to constrain the Planck scaling relation parameters. For this reason, we do not consider the original X-ray+WL calibration reported in table 2 when analysing Planck data. As a baseline, we

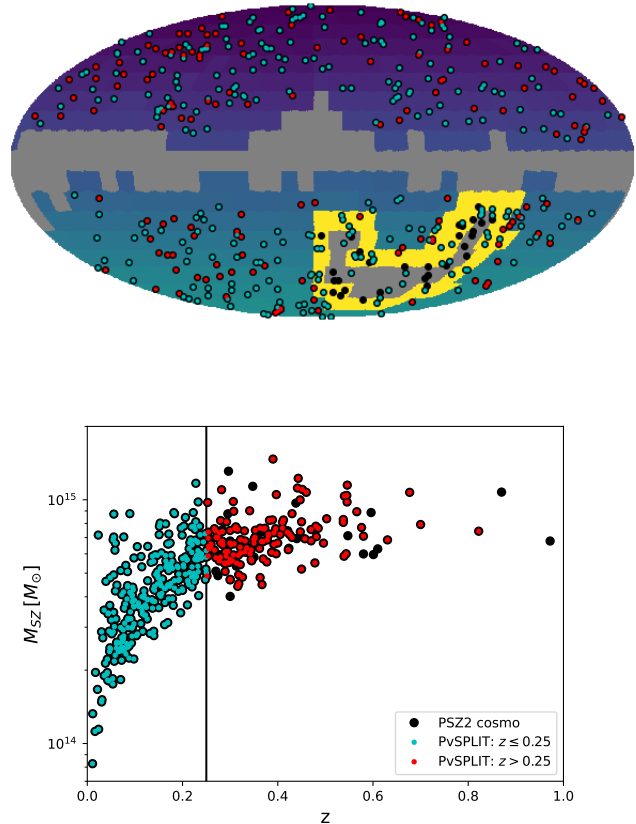


Figure 1. *Upper panel.* Map of Planck patches in galactic coordinates. In grey we show the removed patches, due to the Planck galactic mask and the fully overlapped area with SPT observations. In yellow we highlight the 35 partly overlapping patches between Planck and SPT. *Upper and lower panel.* Comparison between the PSZ2 cosmo catalog (black points), with the PvSPLIT catalog. In the upper panel, we show how the clusters are distributed in the sky. In the lower panel, we show the mass-redshift distribution, considering M_{SZ} mass from Planck Collaboration et al. (2016b). The cyan points are the clusters considered in the $z \leq 0.25$ part of the PvSPLIT likelihood. The red points are the clusters considered in the $z > 0.25$ PvSPLIT likelihood.

use the X-ray calibration for the $\log Y_{\text{SZ}}$ and $\sigma_{\log Y_{\text{SZ}}}$ parameters, as reported in Table 2, and we assume the self-similarity model for the cluster evolution, i.e. $\beta_{\text{SZ}} = 0.66$. We therefore focus the analysis on the constraints that we can obtain on the mass bias and the power-law index of the mass dependence, $(1 - b)_{\text{SZ}}$ and α_{SZ} . We refer to this parameter exploration and likelihood combination as the baseline ‘‘SPTcl + PvSPLIT’’ results. As a further test, we also relax the assumption of redshift self-similar evolution and let the β_{SZ} parameter free to vary.

For the cosmological parameters, we assume a $\nu\Lambda\text{CDM}$ scenario. We vary the following parameters:

Table 3. Redshifts for clusters without redshifts in the original PSZ2 cosmological catalog obtained from photometric (P) or spectroscopic (S) observations.

Cluster	z	Reference
PSZ2 G011.36-72.93	$z = 0.63 \pm 0.04$ (P)	Bleem et al. (2020)
PSZ2 G107.83-45.45	$z = 0.55 \pm 0.05$ (P)	Boada et al. (2019)
PSZ2 G160.83-70.63	$z = 0.24 \pm 0.03$ (P)	Aguado-Barahona et al. (2019)
PSZ2 G237.41-21.34	$z = 0.31 \pm 0.04$ (P)	this work ^a
PSZ2 G293.01-65.78	$z = 0.206 \pm 0.006$ (P)	Klein et al. (2019)
PSZ2 G329.48-22.67	$z = 0.249 \pm 0.001$ (S)	Amodeo et al. (2018)

NOTE—^a from Pan-STARRS (Chambers et al. 2016) following Bleem et al. (2020)

the total matter density Ω_m , the amplitude of primordial curvature perturbation A_s , the Hubble rate h , the baryon density $\Omega_b h^2$, the spectral index for scalar perturbations n_s and the massive neutrino energy density $\Omega_\nu h^2$. When providing the results for the cosmological parameters, we focus also on the σ_8 quantity. We report all the parameters, with the priors used in the analysis, in Table 1. The sampling of the likelihood is performed with the importance nested sampler algorithm `MultiNest` (Feroz et al. 2009), within the `cosmoSIS` package (Zuntz et al. 2015).

As shown in section 2, the halo mass function is a fundamental ingredient for the evaluation of the cluster number counts. For both the SPT and Planck part of the analysis, we make use of the evaluation from Tinker et al. (2008).

3.3. Mass evaluation

We now describe the approach we use to provide a new evaluation of true Planck cluster masses, M_{500} . We follow the discussion in Planck Collaboration et al. (2016b). We start from the Planck cluster observable, the signal-to-noise ratio q , and evaluate $P(M_{500}|q)$, which represents the conditional probability that a cluster with given signal-to-noise ratio q has a mass M_{500} . Following the Bayes theorem, this probability is defined as

$$P(M_{500}|q) \propto P(q|M_{500}) P(M_{500}) \quad (18)$$

where the first term is the conditional probability of the data (the signal-to-noise ratio q), given the model (the cluster mass M_{500}), and the second term is the mass probability distribution. The latter is related to the mass function dN/dM_{500} , such that

$$P(M'_{500}) = \frac{dN/dM_{500}|_{M'_{500}}}{\int dM_{500} dN/dM_{500}}. \quad (19)$$

In order to evaluate $P(q|M_{500})$, we follow the recipe for $P[q|\bar{q}_m(M_{500}, z, l, b)]$, that represents the probability

distribution of the observed signal-to-noise ratio q given the mean one, \bar{q}_m , as already mentioned in section 2. Following Eq. 9, the mean theoretical signal-to-noise ratio is defined as

$$\bar{q}_m \equiv \frac{\bar{Y}_{500}}{\sigma_f(\bar{\theta}_{500}, l, b)}, \quad (20)$$

where \bar{Y}_{500} and $\bar{\theta}_{500}$ are the mean values of the scaling relations defined in Eqs. 14 and 15 and σ_f is the detection filter noise. For fixed values of the cosmological and scaling relation parameters, we have therefore a unique relation between the cluster mass M_{500} and \bar{q}_m .

The probability distribution can be evaluated as

$$P[q|\bar{q}_m(M_{500}, z, l, b)] = \int d \ln q_m \frac{e^{-(q-q_m)^2/2}}{\sqrt{2\pi}} \times \frac{e^{-\ln^2(q_m/\bar{q}_m)/2\sigma_{\ln Y}^2}}{\sqrt{2\pi}\sigma_{\ln Y}}. \quad (21)$$

In the above equation, the second term accounts for the intrinsic scatter of the mass-observable relations, while the first term links the theoretical signal-to-noise ratio q_m to the observed one, assuming pure Gaussian noise.

In practice, we adopt a Monte-Carlo extraction based approach, starting from the parameter space exploration performed for the SPTcl + PvSPLIT analysis. For a given cosmological and scaling relation model, we extract M_{500} in the range $[3 \cdot 10^{13}, 1.2 \cdot 10^{16}] [M_\odot h^{-1}]$ (following what is done in the PvSPLIT likelihood) starting from the mass function distribution. We then evaluate \bar{Y}_{500} , $\bar{\theta}_{500}$ and consequently \bar{q}_m , following Eq. 20.

For the given mean theoretical signal-to-noise ratio, we then extract q_m , following a log-normal distribution with standard deviation equal to the intrinsic mass-observable relation scatter, $\sigma_{\ln Y}$.

Given q_m , we can extract the estimate of the observed signal-to-noise ratio q_{est} , following a Gaussian distribution with standard deviation equal to 1. We then select N values of q_{est} around the corresponding observed

signal-to-noise q , therefore selecting the corresponding values of M_{500} . The posterior distributions for M_{500} are obtained marginalizing over the full parameter space, considering cosmological and scaling relation parameters. The resulting catalog therefore provides the first sample of Eddington-bias-corrected calibrated cluster masses, that include correlations associated with scaling relation and cosmological parameters. As detailed in section 4.2, we make this catalog publicly available.

3.3.1. Mass bias

With the evaluation of M_{500} , we can estimate directly and for each cluster in the PSZ2 sample, the mass bias as $(1-b)_M = M_{SZ}/M_{500}$. We use M_{SZ} estimations provided by the Planck collaboration (Planck Collaboration et al. 2016b) for the 433 clusters in PSZ2, for which the redshift was originally provided.

We highlight the difference between the scaling relation parameter $(1-b)_{SZ}$ entering Eqs. 14 and 15, and the quantity we investigate here. The assumptions of spherical collapse, hydrostatic equilibrium and self-similarity lead to the formulation of Eqs. 14, 15 that link the tSZ observables and the cluster mass. In this case, the mass bias $(1-b)_{SZ}$ is introduced to take into account any generic departure from hydrostatic equilibrium. Nevertheless, as discussed in Planck Collaboration et al. (2016a), M_{SZ} is evaluated as the real cluster mass combining the scaling relation information with the output of the matched filter approach used to detect the clusters. The combination of these different approaches might select cluster scales that do not actually maximise the S/N ratio from the matched filter algorithm, and therefore introduce a further bias in the estimation of the real cluster mass.

We attempt therefore to provide a complete characterisation of the “measured” mass bias $(1-b)_M$, analysing the dependencies with respect to theoretical modelling and observational assumptions.

We consider a mass and redshift evolution for the mass bias. The goal is to understand if we need to further improve the theoretical modelling of the scaling relations. Indeed, as discussed e.g. in Salvati et al. (2019) comparing recent WL mass calibrations (von der Linden et al. 2014; Okabe & Smith 2016; Sereno & Ettori 2015; Smith et al. 2016; Penna-Lima et al. 2017; Sereno et al. 2017; Herbonnet et al. 2020), a correct calibration of the mass bias might need to take into account the mass and redshift distribution of the full cluster catalog.

In addition, we analyse a possible link between the evaluation of the mass bias (and therefore of the cluster mass) and the cluster position in the sky. This dependence might be related to the observational strategy, as

well as to the assumptions for the ingredients used in the matched filter approach. As discussed in section 3.1, the Planck sky area, used for the cluster cosmological analysis, is divided into 417 patches, with each patch having a different value of detection noise $\sigma_f(\theta_{500}, l, b)$. This noise depends on the filter size θ_{500} and is therefore related to the matched filter approach used to detect clusters in the Planck sky. Therefore, the analysis of a possible dependence of the mass bias with respect to the detection noise allows us to quantify the systematic uncertainties coming from the modelling of the whole selection approach.

Considering the mass, redshift and noise dependence, we define the theoretical mass bias $(1-b)_M^{\text{th}}$ as

$$(1-b)_M^{\text{th}} = A_{\text{bias}} \left(\frac{M_{500}}{M_*} \right)^{\gamma_M} \left(\frac{1+z}{1+z_*} \right)^{\gamma_z} \times \left(\frac{\sigma_f(\theta_{500}, l, b)}{\sigma_{f,*}(\theta_{500})} \right)^{\gamma_n} \quad (22)$$

where $M_* = 4.68 \cdot 10^{14} M_\odot$ is the median mass of the sample (obtained from our analysis), $z_* = 0.21$ is the median redshift of the sample and $\sigma_{f,*}(\theta_{500})$ is the median detection noise at the given θ_{500} .

4. RESULTS

In this section we report the results for the combined cosmological analysis of Planck and SPT cluster likelihoods. We also provide an estimate of the cluster mass and mass bias for Planck PSZ2 cosmological sample.

4.1. Cosmological and scaling relation parameters

The results presented in this analysis are obtained combining the full SPT likelihood with the new Planck likelihood, presented in section 2 and 3. We refer to this combination as SPTcl + PvSPLIT. For the baseline analysis we consider the $\nu\Lambda$ CDM scenario. When discussing our results, we focus on the constraints for the cosmological parameters Ω_m and σ_8 and for the Planck scaling relation parameters $(1-b)_{SZ}$ and α_{SZ} . We compare the results for SPTcl + PvSPLIT baseline combination with constraints obtained when considering the SPT data and Planck data alone.

We stress that, when providing results for Planck data alone, we are actually considering the combination of cluster counts with measurements of BAO (Alam et al. 2017; Beutler et al. 2012, 2011; Ross et al. 2015), together with constraints on the baryon density $\Omega_b h^2$ from Big Bang Nucleosynthesis (BBN hereafter). We also consider the full calibration of the scaling relation parameters (as reported in Table 2), following the analysis in Planck Collaboration et al. (2016b). In this work, we

simply perform a new analysis using the `MultiNest` sampler, within the `cosmoSIS` package, in order to provide consistent results. This dataset combination is labelled as “PvFULL”.

We report the constraints on cosmological and scaling relation parameters in Table 4. We show the 68% confidence level (CL hereafter) constraints for all the parameters. In the triangular plot in Fig. 2 we show the one-dimensional and two-dimensional probability distributions for the cosmological and scaling relation parameters.

Table 4. We report the 68% CL constraints on cosmological and scaling relation parameters for different dataset combinations. We refer to the text for the full dataset description.

Parameter	$\nu\Lambda$ CDM		
	SPTcl + PvSPLIT	PvFULL	SPTcl
Ω_m	$0.29^{+0.04}_{-0.03}$	$0.37^{+0.02}_{-0.06}$	0.30 ± 0.03
σ_8	$0.76^{+0.03}_{-0.04}$	$0.71^{+0.05}_{-0.03}$	$0.76^{+0.03}_{-0.04}$
α_{SZ}	$1.49^{+0.07}_{-0.10}$	1.79 ± 0.06	–
$(1 - b)_{SZ}$	$0.69^{+0.07}_{-0.14}$	$0.76^{+0.07}_{-0.08}$	–

From these results, we see that SPT cluster data are driving the constraining power, as it is shown from the shift of Ω_m contours towards lower values and σ_8 contours towards larger values for the SPTcl + PvSPLIT baseline combination, with respect to PvFULL constraints. We stress again that for the SPTcl + PvSPLIT baseline combination we are not including BAO+BBN dataset and part of the X-ray+WL mass calibrations when considering Planck data, therefore losing part of the constraining power that leads to the tight bounds obtained for the PvFULL analysis.

As a reference, we show in Fig. 6, in Appendix A, a comparison between PvFULL and the same Planck data without adding external datasets and external calibrations for the scaling relations, following the approach we use when analysing PvSPLIT. From this comparison, we clearly see the significant impact of SPT data in constraining cosmology and the mass-calibration.

We now focus on the Planck scaling relation parameters $(1 - b)_{SZ}$ and α_{SZ} . Regarding the mass bias, we find $(1 - b)_{SZ} = 0.69^{+0.07}_{-0.14}$. Although pointing towards low value of $(1 - b)$, this result is still consistent with constraints obtained from recent WL calibration and numerical simulation analyses, see e.g. a collection of re-

sults in Salvati et al. (2018); Gianfagna et al. (2021). Nevertheless, not considering the WL calibration from the CCCP analysis (used in the original Planck analysis) leads to a slight enlargement in the constraints.

Regarding the mass slope α_{SZ} , we find $\alpha_{SZ} = 1.49^{+0.07}_{-0.10}$, which is $\sim 4\sigma$ away with respect to the value obtained when adopting the X-ray calibration, $\alpha_{SZ} = 1.79 \pm 0.06$. We recall here that, following the definition of the scaling relations in Eqs. 14 and 15, the value of $\alpha_{SZ} \simeq 1.8$ is in agreement with self-similarity assumption.

The shift we find seems to be due to a combination of different effects. First of all, the PvSPLIT likelihood provides slightly different constraints with respect to the original PvFULL one, especially on the α_{SZ} parameter, already pointing to $1.71^{+0.07}_{-0.09}$, as shown in Fig. 7 and in Table 8, in Appendix A.

We then test for the possible impact of sampling choice. In particular, as discussed also in Bocquet et al. (2019), sampling on A_s or on $\ln(10^{10}A_s)$ provides different constraints on the cosmological parameters, where the main effect can be seen on Ω_m and H_0 . In our SPTcl + PvSPLIT baseline analysis we are following Bocquet et al. (2019) and sampling linearly on A_s . In the original Planck analysis, the sampling is done on $\ln(10^{10}A_s)$, as it is also done for the PvFULL results. We test therefore what happens when considering a logarithmic sampling for the SPTcl + PvSPLIT combination. The results are reported in Appendix A, in Table 8 and Fig. 8 (pink contours). In this case, for the SPTcl + PvSPLIT + $\ln A_s$ combination, we find a negligible impact when considering the Ω_m and σ_8 constraints. We find a larger effect when focusing on the scaling relation parameters. In particular, the constraints for the mass slope are $\alpha_{SZ} = 1.60^{+0.10}_{-0.18}$, being therefore consistent with both the original PvFULL value and the baseline SPTcl + PvSPLIT results.

Nevertheless, the main cause for the departure from self-similarity in the mass slope of the scaling relations is due to the lower value of Ω_m obtained for the SPTcl + PvSPLIT combination, as it can be seen in Fig. 2.

As an additional note, we stress that when focusing on the SPT scaling relation parameters (described in Eqs. 6-8), results for the SPTcl + PvSPLIT combination are fully consistent with the original analysis presented in Bocquet et al. (2019).

As a final test, we relax the assumption of self-similarity for the redshift evolution of the scaling relations, therefore adding β_{SZ} as a varying parameter. We report the constraints for the cosmological and scaling relation parameters in Table 8 and Fig. 8 (black contours), in Appendix A. We find these results to be fully

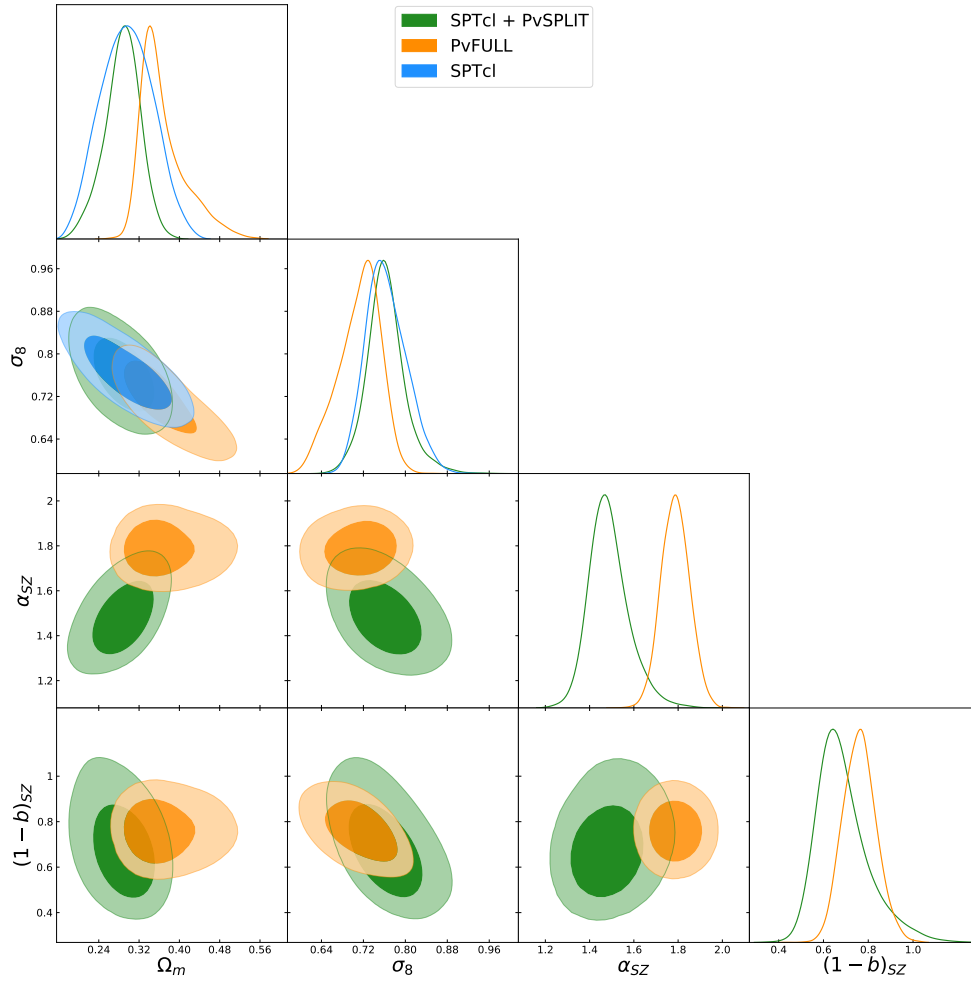


Figure 2. We show the one-dimensional and two-dimensional probability distributions for the cosmological (Ω_m , σ_8) and Planck scaling relation (α_{SZ} , $(1-b)_{SZ}$) parameters. The contours represent the 68% and 95% CL. We compare results for different dataset combinations: SPTcl + PvSPLIT in green (baseline results of this analysis), PvFULL in orange and SPTcl in blue. We refer to the text for the complete description of the datasets.

in agreement with our baseline analysis. For the redshift evolution parameter, we find $\beta_{\text{SZ}} = 0.57_{-0.51}^{+0.20}$, in agreement with the predicted self-similar value $\beta_{\text{SZ}} = 2/3$.

As a reference, in Fig. 8 we show also the latest results for Planck CMB in the $\nu\Lambda\text{CDM}$ scenario from Planck Collaboration et al. (2020a).

4.2. Mass and mass bias evaluation

We now present the results for the mass evaluation analysis for the 439 clusters in the Planck cosmological cluster sample.

We start considering the full sample of cosmological and scaling relation parameters. We make use of the results for the SPTcl + PvSPLIT baseline presented in the previous section, evaluating M_{500} and $P(M_{500}|g)$ for each step of the chain. The posterior distributions for the cluster masses are therefore obtained marginalising over the cosmological and scaling relation parameters.

In Fig. 3 we show the results obtained from the Monte-Carlo extraction, presenting the evaluated M_{500} as a function of redshift. These results well reproduce the Planck selection threshold, being able to detect low-mass objects only in the low-redshift regime. The full cluster mass catalog is available at https://pole.uchicago.edu/public/data/sptplanck_cluster. We report the first entries in Table 5: in the sixth column we report the constraints on M_{500} and in the seventh column we report the full array of masses extracted through the Monte Carlo approach. We note that, for the 27 clusters in common with the SPT-SZ catalog, our mass estimation is in agreement within 2σ with the estimates from Bocquet et al. (2019), as further discussed in Appendix B.

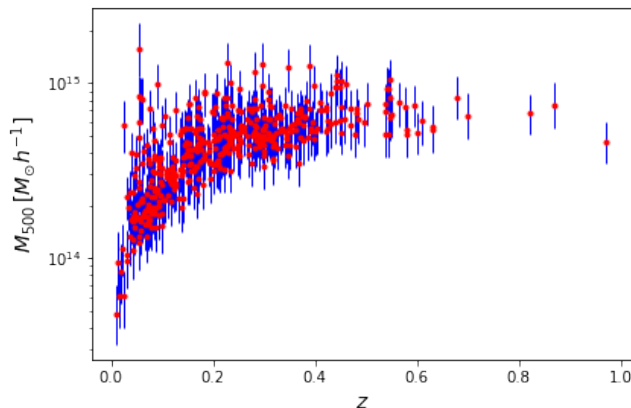


Figure 3. Cluster masses for the Planck cosmological sample, evaluated with a Monte-Carlo extraction approach. We show the best-fit value (red points) and the 68% c.l. errors (in blue).

We now compare the M_{500} evaluated masses, with the M_{SZ} masses obtained from the Planck catalog. In this case, we restrict the analysis to the 433 clusters for which we have the M_{SZ} estimation. We provide therefore a direct evaluation of the mass bias for each cluster in the considered sample, following the definition $(1-b)_M = M_{\text{SZ}}/M_{500}$.

We analyse the possible redshift, mass and noise dependence for the mass bias $(1-b)_M$, as defined in Eq. 22. We report these trends in Fig. 4 and the results for the fit in Table 6. While we find a value for the amplitude that is consistent with the constraints for $(1-b)_{\text{SZ}}$, having $A_{\text{bias}} = 0.69_{-0.09}^{+0.04}$, we find also strong evidence for mass and redshift evolution. In particular, the mass bias is increasing for high redshift and low mass, with $\gamma_M = -0.41_{-0.06}^{+0.04}$ and $\gamma_z = 0.81 \pm 0.13$. Regarding the detection noise, we find no evidence for the mass bias to be dependent in this quantity, since we have γ_n consistent with 0 within 1σ .

We conclude this section presenting masses for the PSZ2 cosmo catalog obtained when fixing the cosmological and scaling relation parameters. For the cosmological parameters, we adopt a flat $\nu\Lambda\text{CDM}$ scenario, following Bocquet et al. (2019). For the Planck scaling relation parameters, we take the best-fit values from the SPTcl + PvSPLIT baseline run with the fixed cosmology. The values of the parameters are reported in Table 7. Also in this case, the full cluster mass catalog is available at https://pole.uchicago.edu/public/data/sptplanck_cluster. We report the first entries in Table 5, eight column. As for the marginalised masses, for the 27 clusters in common with the SPT-SZ catalog, our mass estimation is in agreement within 2σ with the estimates from Bocquet et al. (2019), as further discussed in Appendix B.

We show in Fig. 5 the Planck evaluated masses M_{500} , as function of redshift, in comparison with cluster masses from the SPT-SZ 2500 deg² catalog (Bocquet et al. 2019). As a reference, we also add clusters from recent SPT observations: the 79 clusters from the SPT-pol 100 deg² sample (Huang et al. 2020), and the 448 clusters from the SPTpol Extended (SPT-ECS) sample (Bleem et al. 2020).

5. DISCUSSION

The characterization and calibration of the scaling relations between survey observables and cluster mass is a non-negligible issue in current cluster cosmology, see e.g Pratt et al. (2019) for a comprehensive review. The use of multi-wavelength data is fundamental in order to provide mass estimation.

Table 5. First entries for the new Planck cluster catalog. We report cluster ID, coordinates, redshift and signal-to-noise ratio as delivered by Planck collaboration. We add in the sixth and seventh column the evaluation of M_{500} obtained marginalising over cosmological and scaling relation parameters from our SPTcl+PvSPLIT analysis (labelled as “free”), and the full array of extracted masses (labelled as “free,c”). In the eight column we report the evaluation of M_{500} for the fixed values of cosmological and scaling relation parameters reported in Table 7 (labelled as “fixed”). The full catalog is available at https://pole.uchicago.edu/public/data/sptplanck_cluster.

Planck ID ^a	ra ^a	dec ^a	z ^a	S/N ^a	$M_{500}^{\text{free}} [10^{14} M_{\odot} h^{-1}]$	$M_{500}^{\text{free,c}} [10^{14} M_{\odot} h^{-1}]$	$M_{500}^{\text{fixed}} [10^{14} M_{\odot} h^{-1}]$
PSZ2 G000.04+45.13	229.19051	−1.01722	0.1198	6.75319	$3.37^{+0.88}_{-1.11}$	[2.60, ..., 4.24]	$3.80^{+0.34}_{-1.04}$
PSZ2 G000.13+78.04	203.55868	20.25599	0.171	9.25669	$4.52^{+1.11}_{-1.27}$	[3.40, ..., 5.38]	$5.65^{+0.91}_{-0.54}$
PSZ2 G000.40-41.86	316.0699	−41.33973	0.1651	8.57995	$4.25^{+1.07}_{-1.26}$	[2.85, ..., 5.0]	$5.00^{+0.65}_{-0.83}$
PSZ2 G000.77-35.69	307.97284	−40.59873	0.3416	6.58179	$5.31^{+1.43}_{-1.57}$	[3.32, ..., 3.92]	$5.81^{+0.90}_{-1.20}$
PSZ2 G002.77-56.16	334.65947	−38.87941	0.1411	9.19606	$3.75^{+0.92}_{-1.10}$	[2.90, ..., 5.52]	$4.18^{+0.29}_{-1.00}$

NOTE—^afrom Planck Legacy Archive (<https://pla.esac.esa.int>)

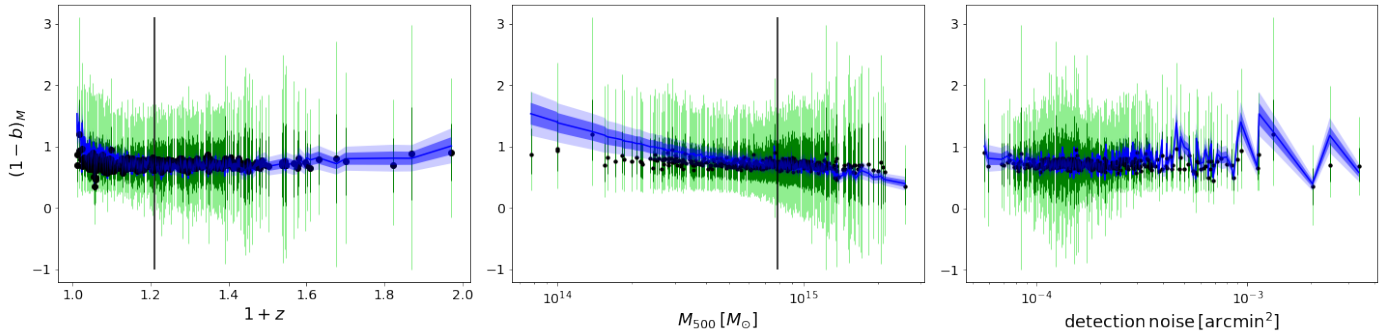


Figure 4. Mass bias evaluated from the Monte-Carlo extracted masses M_{500} , $(1-b)_M = M_{SZ}/M_{500}$. We show the mass bias as a function of redshift (left panel), M_{500} (middle panel) and detection noise (right panel): we report the best-fit (black points) with 68% (dark green) and 95% (light green) error bars. The blue shaded area represents the trend and the 68% and 95% CL obtained when fitting Eq. 22, following results in Table 6. The black vertical lines show the values of z_* and M_* .

Table 6. Parameters for the mass, redshift and detection noise dependence of the mass bias. We report the 68% CL constraints.

Parameter	Value	Parameter	Value
A_{bias}	$0.69^{+0.04}_{-0.09}$	γ_z	0.81 ± 0.13
γ_M	$-0.41^{+0.04}_{-0.06}$	γ_n	$0.05^{+0.06}_{-0.08}$

Table 7. Fixed values of cosmological and Planck scaling relation parameters used to evaluate cluster masses.

Parameter	Value	Parameter	Value
Ω_m	0.3	α_{SZ}	1.62
σ_8	0.8	β_{SZ}	0.67
$\Omega_\nu h^2$	0.00064	$\sigma_{\ln Y, SZ}$	0.07
$\log Y_*$	−0.14	$(1-b)_{SZ}$	0.58

Planck and SPT analyses make use of X-ray and WL measurements to calibrate the scaling relations, with different approaches. The SPT analysis is based on a multi-observable likelihood: the gas mass and spectroscopic temperature (X-ray data) and the shear profiles and redshift distributions (WL data) are added directly into the

cosmological analysis, and have been measured for clusters within the SPT sample using dedicated follow-up observations.

The Planck analysis is based on external calibrations: constraints on the scaling relation parameters are ob-

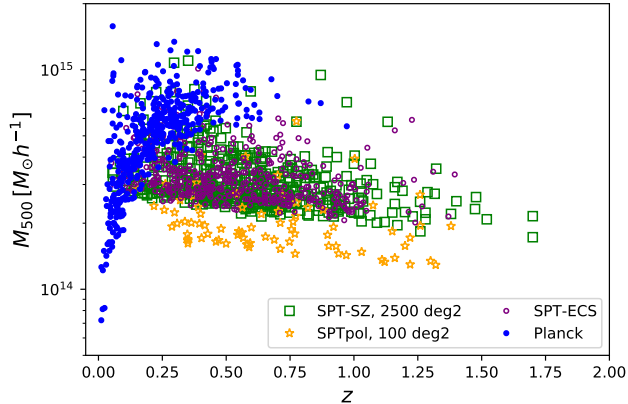


Figure 5. Evaluation of cluster masses, for each cluster in the Planck cosmological cluster sample (blue points), for fixed values of cosmological and scaling relation parameters. We report also the SPT cluster masses from the SPT-SZ 2500 deg² catalog (green squares), from the SPTpol 100 deg² catalog (yellow stars) and from the SPTpol Extended cluster catalog (purple circles).

tained through Gaussian priors derived from the external analyses. In particular, for the calibration of the mass bias, $(1 - b)$ parameter, several WL analyses came out in the last years, apart from the CCCP baseline value used in Planck Collaboration et al. (2016b). These works provide different results, depending on the different approaches and the considered PSZ2-cosmo cluster subsample, see e.g. von der Linden et al. (2014); Okabe & Smith (2016); Sereno & Ettori (2015); Smith et al. (2016); Penna-Lima et al. (2017); Sereno et al. (2017); Herbonnet et al. (2020). We stress that all these analysis are based on very small subsamples (few tens of clusters) of the full PSZ2-cosmo cluster catalog.

There have been also attempts to estimate Planck cluster masses through CMB lensing, as done in Melin & Bartlett (2015); Zubeldia & Challinor (2019). Furthermore, in recent years several analyses from hydrodynamical simulations computed estimates of the mass bias $(1 - b) \sim 0.8$, see a collection of results in Salvati et al. (2018); Gianfagna et al. (2021).

It has been largely discussed in Planck Collaboration et al. (2016b) that different values for the mass bias induce non negligible shifts in the cosmological parameter constraints, with $(1 - b)$ showing the largest correlation with the σ_8 parameter. Through this degeneracy it is also possible to evaluate the mass bias combining cluster counts with CMB primary anisotropies. Latest results from Planck collaboration still push towards very low values of the mass bias, finding $(1 - b) = 0.62 \pm 0.03$ (Planck Collaboration et al. 2020a), still in tension with other WL and numerical simulation estimations. We

recall here that $(1 - b) \sim 0.6$ is in tension also with astrophysical evaluations, since it results in a too low value for the universal gas fraction, as discussed e.g. in the X-COP analysis (Eckert et al. 2019).

The mass calibration problem is therefore linked to the well-known σ_8 tension between galaxy clusters and CMB cosmology. Even though cosmological parameters provided by Planck cluster counts and CMB primary anisotropies are now fully in agreement within 2σ , as shown in Salvati et al. (2018); Planck Collaboration et al. (2020a), CMB pushing the mass bias towards lower values might still be a sign of discrepancy between high redshift and low redshift Universe. It is therefore fundamental to further analyse the mass calibration impact in the cosmological analysis.

The aim of this work is to provide a completely independent evaluation for the Planck scaling relation parameters, without relying on priors from external calibrations. We exploit the cosmological constraining power of SPT-SZ cluster catalog, with its internal WL mass calibration, and use the Planck-SPT combination to obtain our results.

We start focusing on the results obtained for the SPTcl + PvSPLIT cluster catalog combination, presented in the previous section. First of all, we highlight the powerful cosmological constraining power of the SPT-SZ cluster sample: SPT data are driving the results, pushing the constraints for the SPTcl + PvSPLIT combination. For this dataset combination, we are also able to get tight constraints on the Planck scaling relation parameters, comparable with the results from Pv-FULL (i.e. the original full Planck likelihood), as shown in Table 4. In particular, we decide to focus on the parameters describing the mass dependence, therefore not considering external calibration and assumption of self-similarity for the mass bias, described by $(1 - b)_{SZ}$, and the mass slope α_{SZ} .

For the mass bias, we find $(1 - b)_{SZ} = 0.69^{+0.07}_{-0.14}$. This is still in agreement within 2σ with the different external WL calibrations and hydro-dynamical simulation estimations, but it also encompasses the lower values preferred from CMB data. This result can be further discussed in light of the evaluation of $(1 - b)_M$ that we performed for each single cluster. We discuss in section 3.3.1 the difference between the scaling relation parameter and the measured mass bias. The two quantities describe from different approaches a general non-precise knowledge of how the astrophysical processes affect the theoretical model for the cluster evolution (and as a consequence how we model the mass-observable relation and the selection approach). By analysing $(1 - b)_M$, we find strong hints for mass and redshift evolution of this quan-

tity, with the amplitude being consistent with $(1-b)_{\text{SZ}}$, having $A_{\text{bias}} = 0.69_{-0.09}^{+0.04}$, as shown in Table 6. The increasing trend for the redshift evolution is also consistent with the analysis shown in Salvati et al. (2019).

We now focus on the mass slope of the scaling relations, α_{SZ} . For SPTcl + PvSPLIT we find $\alpha_{\text{SZ}} = 1.49_{-0.10}^{+0.07}$, which is $\sim 4\sigma$ lower than the self-similarity value. As discussed in section 4.1, this low value is due to a combination of different effects, with the dominant one being the shift of Ω_m towards lower values. Indeed, this shift slightly tilts the mass function, such that it leads to fewer objects at low mass and more objects in the high-mass tail. The low value of α_{SZ} seems to accommodate for this tilt, balancing the low-mass high-mass weight. The mass-redshift evolution of $(1-b)_M$ seems to account for the same effect, balancing the low-mass high-mass trend. We also stress that, when not assuming self-similarity for the redshift evolution of Planck scaling relation and sampling also on the β_{SZ} parameter, we find consistent results with the baseline analysis and no evidence for departure from self-similarity.

From these combined results on the Planck scaling relation parameters and the estimated mass bias, we can take one main message: the simple model for the mass calibration of tSZ clusters, based on the assumptions of self-similarity, spherical symmetry and hydrostatic equilibrium, needs to be improved towards a more realistic description, at least for the modelling of the mass (and therefore scale) dependence. This is indeed the approach used for the SPT-SZ cluster analysis: the empirical, multi-observable approach used for the mass calibration provides constraints for the different parameters (defined in Eqs.6-8) not relying on strong theoretical assumptions.

As a last point, we discuss the dependence of the measured mass bias with respect to the detection noise. As described in section 3.3.1, with this parameterization we try to quantify the impact of the detection process in the full cosmological modelling. From our analysis, we find no hint for a noise dependence of the mass bias, having $\gamma_n = 0.05_{-0.08}^{+0.06}$. As a further test, we check the results when considering only the noise dependence for the bias, i.e.

$$(1-b)_M^{\text{th}} = A_n \left(\frac{\sigma_{\text{f}}(\theta_{500}, l, b)}{\sigma_{\text{f},*}(\theta_{500})} \right)^{\gamma_n}. \quad (23)$$

In this case, we find $A_n = 0.60_{-0.14}^{+0.06}$ and $\gamma_n = -0.37_{-0.12}^{+0.14}$, pointing to a decreasing trend of the measured bias with respect to the noise. This implies that the M_{SZ} estimation for clusters detected in patches with higher detection noise is more biased, possibly due to a loss of tSZ signal.

On the other hand, when considering only the mass and redshift dependence for the measured mass bias, we find results for the amplitude and the slopes that are fully consistent with what we report in Tab. 6. This stresses even more that an incorrect characterization of the mass and redshift dependence for the mass-observable relation is still a dominant source of uncertainties with respect to possible systematics coming from the modelling of the cluster selection process.

6. CONCLUSION

In this paper we provide the first combination of Planck and SPT cluster catalogs for a cosmological analysis, with the aim of exploiting the SPT cosmological constraining power to provide an independent evaluation of Planck scaling relation parameters. We build a new likelihood (labelled ‘‘PvSPLIT’’) to analyse the Planck PSZ2 cosmo sample, removing the clusters and sky patches in common with SPT observations.

The baseline analysis is given by the ‘‘SPTcl + PvSPLIT’’ combination, where we do not use the previously employed external X-ray and WL calibrations for the mass slope α_{SZ} and the mass bias $(1-b)_{\text{SZ}}$ for the Planck scaling relations.

We summarize our main findings below:

1. We show the strong constraining power of SPT-SZ clusters, which drives the results for the SPTcl + PvSPLIT combination. Focusing on Planck scaling relation parameters, we find that the SPTcl + PvSPLIT combination provides results comparable in accuracy with the external X-ray and WL calibrations used for the original Planck analysis, having $\alpha_{\text{SZ}} = 1.49_{-0.10}^{+0.07}$ and $(1-b)_{\text{SZ}} = 0.69_{-0.14}^{+0.07}$. We stress that the value of α_{SZ} that we find is $\sim 4\sigma$ lower than the expected self-similar value, $\alpha_{\text{SZ}} = 1.8$. This seems to be mainly due to the lower values of Ω_m preferred from SPT data.
2. Through a Monte Carlo extraction approach, we provide new estimates of Planck cluster masses M_{500} , obtained marginalising over cosmological and scaling relation parameters from the SPTcl + PvSPLIT analysis. We provide also an evaluation of M_{500} masses for Planck clusters in the PSZ2 cosmo catalog at fixed values of cosmological and scaling relation parameters. The cluster mass catalogs are available at https://pole.uchicago.edu/public/data/sptplanck_cluster.
3. We provide a measurement of the mass bias, $(1-b)_M$, for 433 over 439 clusters of the PSZ2 cosmo sample (for which we have an estimation

of M_{SZ}), using our estimation of M_{500} marginalized over cosmological and scaling relation parameters. In evaluating $(1 - b)_M$, we study a possible dependence with respect to the cluster mass and redshift, and to the survey detection noise. The aim is to highlight the impact, in the cosmological analysis, of the assumed modelling for the mass-observable relation and the cluster detection approach. On the one hand, we find $(1 - b)_M$ to have a decreasing trend with respect to the cluster mass and an increasing trend with respect to redshift, with the slopes being $\gamma_M = -0.41^{+0.04}_{-0.06}$ and $\gamma_z = 0.81 \pm 0.13$. On the other hand, we do not see any noise dependence, having γ_n fully consistent with 0.

4. Comparing the results for the scaling relation parameters and the measured mass bias dependencies, we find them to mimic the same effects, mainly a departure from self-similarity for the cluster evolution, and therefore a necessity to different dependencies for the low-mass vs. high-mass and low-redshift vs. high-redshift clusters.

This analysis confirms the importance of an accurate mass calibration when using galaxy clusters for the cosmological analysis. We find that the simple model for the mass calibration of tSZ clusters, based on the assumptions of self-similarity, spherical symmetry and hydrostatic equilibrium, needs to be improved towards a more realistic description. Furthermore, we stress that the adopted modelling should take into the cluster sample selection, from the cluster mass-redshift distribution to the impact of the detection approach.

ACKNOWLEDGMENTS

LS and MC are supported by ERC-StG "Cluster-sXCosmo" grant agreement 716762. AS is supported by the ERC-StG 'ClustersXCosmo' grant agreement 716762 and by the FARE-MIUR grant 'ClustersXEuclyd' R165SBKTMA and INFN InDark Grant. TS acknowledges support from the German Federal Ministry for Economic Affairs und Energy (BMWi) provided through DLR under projects 50OR2002 and 50OR2106, as well as support provided by the Deutsche Forschungsgemeinschaft (DFG, German Research Foundation) under grant 415537506. The Melbourne group acknowledges support from the Australian Research Council's Discovery Projects scheme (DP200101068). This research made use of: computation facilities of CINECA, within the projects INA17_C5B32, INA20_C6B51, INA21_C8B43, and at the Observatory of Trieste (Taffoni et al. 2020; Bertocco et al. 2020); observations obtained with Planck (<http://www.esa.int/Planck>), an ESA science mission with instruments and contributions directly funded by ESA Member States, NASA, and Canada; the SZ-Cluster Database (<http://szcluster-db.ias.u-psud.fr>) operated by the Integrated Data and Operation Centre (IDOC) at the Institut d'Astrophysique Spatiale (IAS) under contract with CNES and CNRS.

The South Pole Telescope program is supported by the National Science Foundation (NSF) through grants PLR-1248097 and OPP-1852617. Partial support is also provided by the NSF Physics Frontier Center grant PHY-1125897 to the Kavli Institute of Cosmological Physics at the University of Chicago, the Kavli Foundation, and the Gordon and Betty Moore Foundation through grant GBMF#947 to the University of Chicago. Argonne National Laboratory's work was supported by the U.S. Department of Energy, Office of Science, Office of High Energy Physics, under contract DE-AC02-06CH11357. *Facilities:* Magellan: Clay (Megacam), Hubble Space Telescope, Chandra, Gemini:South (GMOS), Magellan: Clay (PISCO).

APPENDIX

A. FURTHER ANALYSIS

We report here results for different dataset combinations, in the $\nu\Lambda$ CDM scenario, in order to further discuss the constraints presented in section 4.1. We start considering different dataset combinations when analysing the Planck cluster data. In particular, we compare results for the "PvFULL" likelihood with results obtained considering Planck data only. Following Planck Collaboration et al. (2016b), the "PvFULL" likelihood is given by the combination of the Planck cluster cosmological catalog, with external X-ray and WL calibrations, BAO data (Alam et al. 2017; Beutler et al. 2012, 2011; Ross et al. 2015) and BBN constraints on the baryon density. In Fig. 6 we show the impact of not considering external datasets and X-ray and WL calibrations on the mass bias and mass slope of the scaling relations.

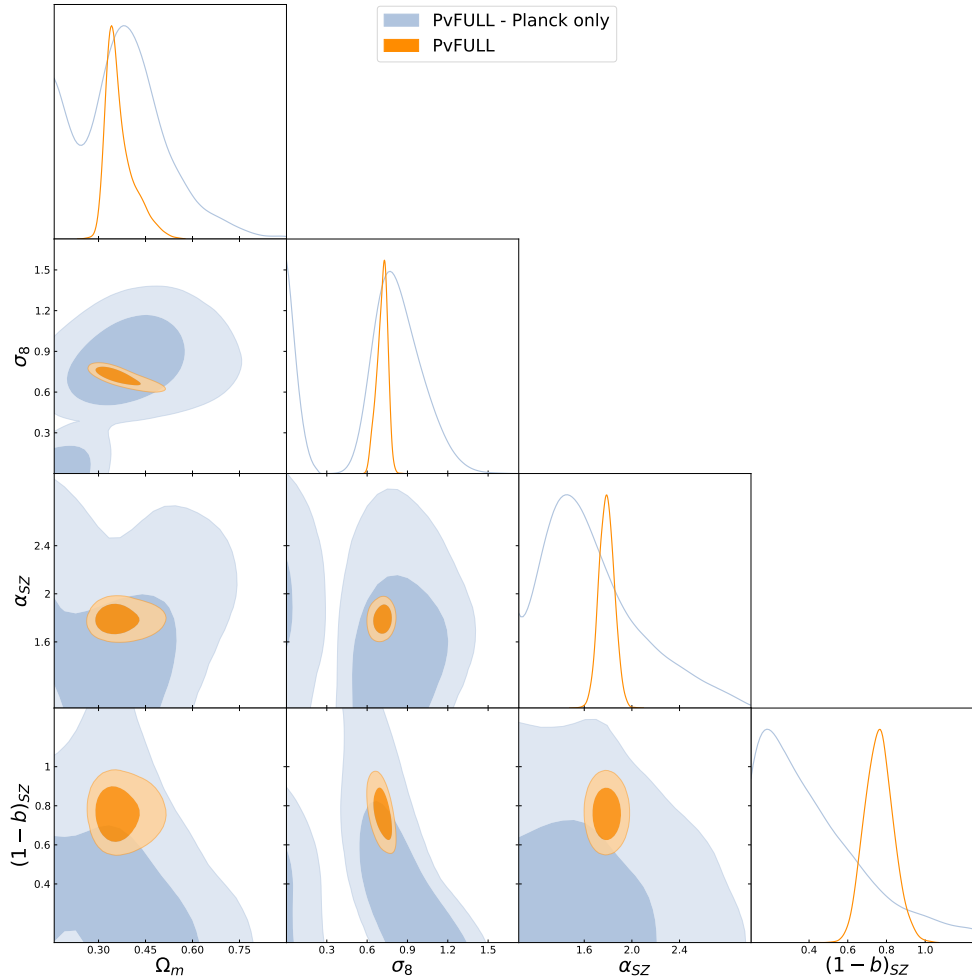


Figure 6. We show the one-dimensional and two-dimensional probability distributions for the cosmological (Ω_m , σ_8) and Planck scaling relation (α_{SZ} , $(1-b)_{SZ}$) parameters. The contours represent the 68% and 95% CL. We compare results for the complete Planck analysis (Planck clusters + BAO + BBN + external scaling relation calibrations assuming self-similar redshift evolution) in orange, with results obtained considering only Planck clusters (light blue).

We now compare the results between the original Planck PvFULL likelihood with the new formulation provided in this work (PvSPLIT), in the $\nu\Lambda$ CDM scenario. For this comparison, in both cases we consider the full external X-ray and WL calibration of the scaling relations and we add BAO and BBN as external datasets. We show the results in Fig. 7 and in Table 8.

We conclude this section showing the results for the SPTcl + PvSPLIT dataset combination when considering the logarithmic sampling of the A_s parameter and when relaxing the assumption of self-similarity for the redshift evolution of the scaling relations, as discussed in section 4.1. Results are shown in Fig. 8 (pink and black contours respectively) and in Table 8, compared with the baseline analysis discussed in section 4.1. We also show the constraints from the latest Planck CMB analysis (Planck Collaboration et al. 2020a) (brown contours). The MCMC chains are taken from the Planck Legacy Archive¹.

B. MASS COMPARISON

We compare the cluster masses for the 27 clusters in common between Planck and SPT-SZ cosmological catalog, for redshift $z > 0.25$. For the SPT-SZ masses, we consider estimates from Bocquet et al. (2019) available on the SPT webpage². For the Planck masses, we make use of our Monte-Carlo estimates. In Fig. 9 we show the quantity

¹ <https://pla.esac.esa.int>

² <https://pole.uchicago.edu/public/data/sptsz-clusters/>

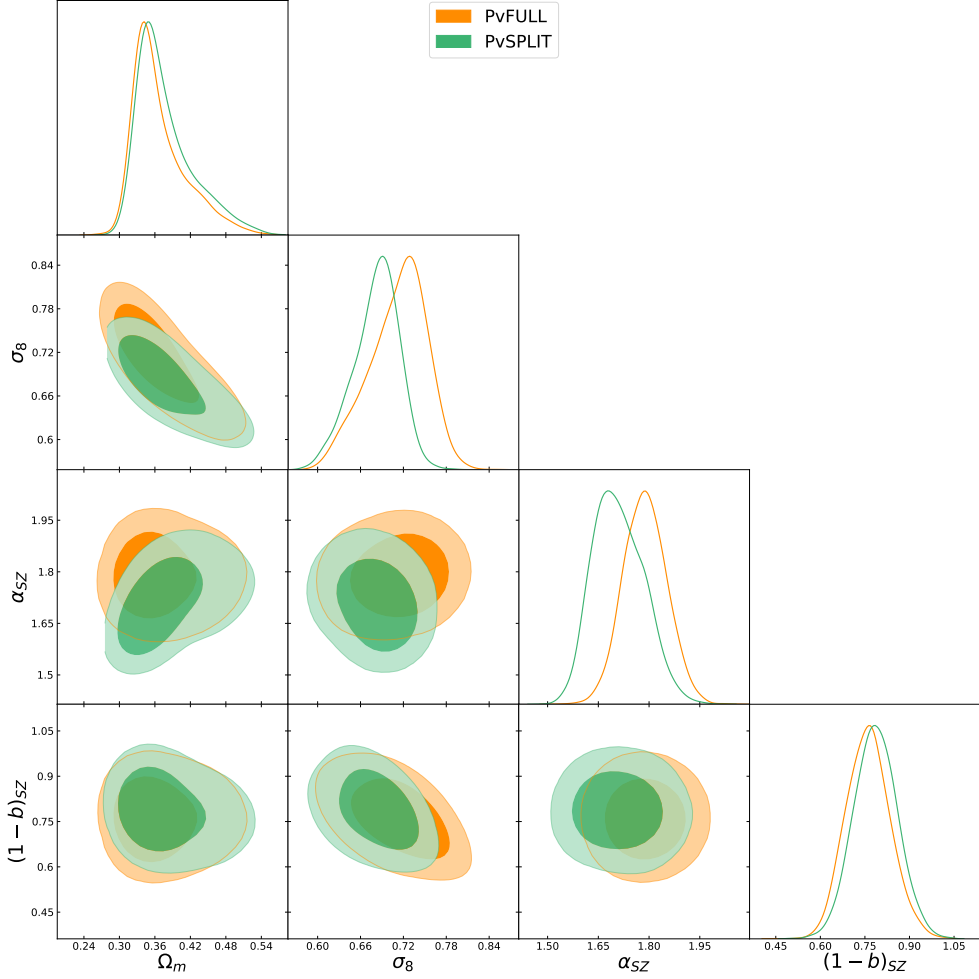


Figure 7. We show the one-dimensional and two-dimensional probability distributions for the cosmological (Ω_m , σ_8) and Planck scaling relation (α_{SZ} , $(1-b)_{SZ}$) parameters. The contours represent the 68% and 95% CL. We compare results for the original Planck analysis (Planck clusters + BAO + BBN + external scaling relation calibrations assuming self-similar redshift evolution) in orange (PvFULL), with results obtained considering the new Planck likelihood PvSPLIT (light green).

Table 8. We report the 68% CL constraints on cosmological and scaling relation parameters for different dataset combinations. We refer to the text for the full dataset description.

Parameter	$\nu\Lambda$ CDM					
	SPTcl + PvSPLIT	PvFULL	SPTcl	PvSPLIT	SPTcl + PvSPLIT + $\ln A_s$	SPTcl + PvSPLIT + β_{SZ}
Ω_m	$0.29^{+0.04}_{-0.03}$	$0.37^{+0.02}_{-0.06}$	0.30 ± 0.03	$0.38^{+0.02}_{-0.06}$	$0.30^{+0.03}_{-0.04}$	$0.28^{+0.03}_{-0.04}$
σ_8	$0.76^{+0.03}_{-0.04}$	$0.71^{+0.05}_{-0.03}$	$0.76^{+0.03}_{-0.04}$	$0.68^{+0.04}_{-0.03}$	0.75 ± 0.03	0.77 ± 0.04
H_0	$61.3^{+1.3}_{-6.3}$	$71.0^{+1.6}_{-4.0}$	$61.5^{+2.6}_{-6.0}$	$71.2^{+1.7}_{-4.0}$	$69.4^{+5.9}_{-14.4}$	$61.8^{+1.3}_{-6.8}$
α_{SZ}	$1.49^{+0.07}_{-0.10}$	1.79 ± 0.06	—	$1.71^{+0.07}_{-0.09}$	$1.60^{+0.10}_{-0.18}$	$1.48^{+0.07}_{-0.10}$
$(1-b)_{SZ}$	$0.69^{+0.07}_{-0.14}$	$0.76^{+0.07}_{-0.08}$	—	0.79 ± 0.07	$0.74^{+0.09}_{-0.16}$	$0.71^{+0.08}_{-0.14}$
β_{SZ}	0.67	0.67	—	0.67	0.67	$0.57^{+0.20}_{-0.51}$

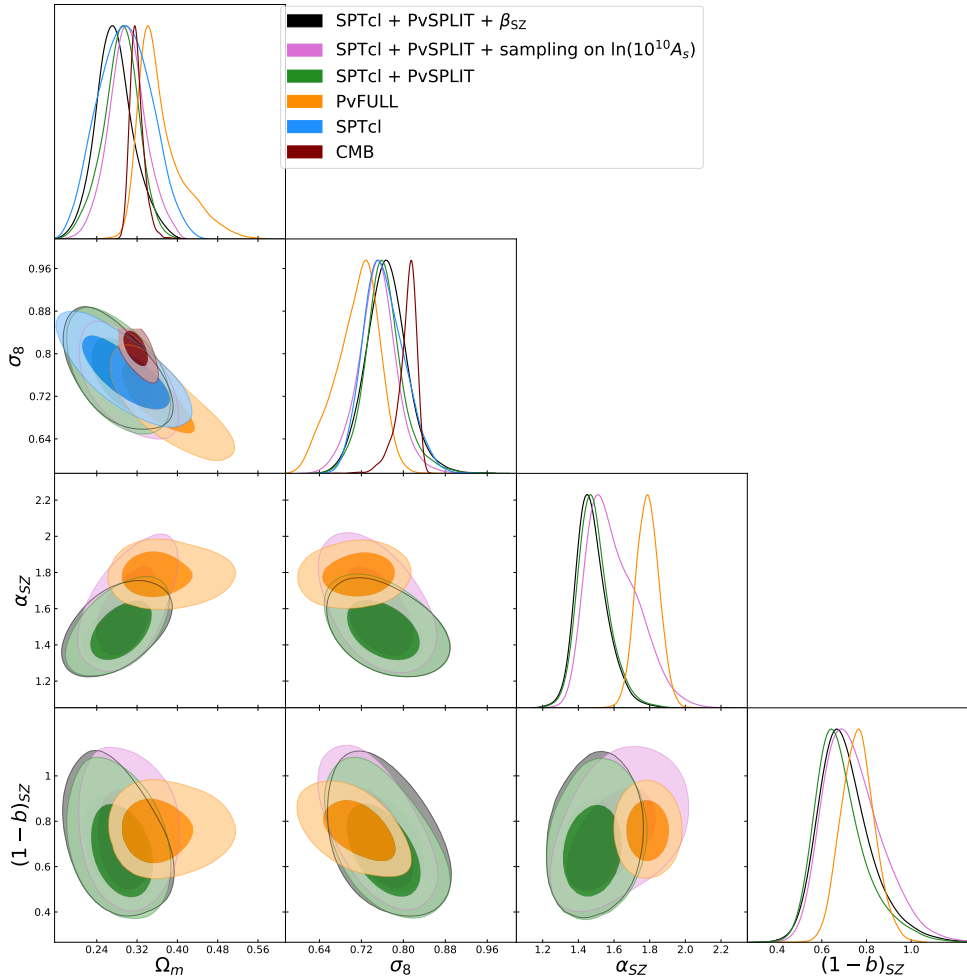


Figure 8. We show the one-dimensional and two-dimensional probability distributions for the cosmological (Ω_m , σ_8) and Planck scaling relation (α_{SZ} , $(1-b)_{SZ}$) parameters. The contours represent the 68% and 95% CL. We compare results for different dataset combinations, as described in the text.

$\Delta_M = (M_{500,P} - M_{500,S})/\sigma$, where we define $\sigma = \sqrt{\sigma_{\text{Planck}}^2 + \sigma_{\text{SPT}}^2}$. We consider the mass estimates obtained marginalising over cosmological and scaling relation parameters (in blue, top panels) and fixing the parameters (in black, bottom panels). We note that the values are quite spread, nevertheless showing a consistency within 2σ between the different estimations. The agreement is stronger for the marginalised estimates, $\Delta_M = 0.37 \pm 0.69$, than for estimations at fixed cosmological and scaling relation parameters, $\Delta_M = 1.25 \pm 1.41$.

As a further test, we show the comparison between Planck M_{SZ} masses from [Planck Collaboration et al. \(2016b\)](#) and the SPT marginalised masses, in Fig. 10. In this case we find $\Delta_M = -2.20 \pm 2.22$, clearly showing that M_{SZ} estimations are biased low.

REFERENCES

- Abbott, T. M. C., et al. 2020, *Phys. Rev. D*, 102, 023509, doi: [10.1103/PhysRevD.102.023509](https://doi.org/10.1103/PhysRevD.102.023509)
- Adami, C., Giles, P., Koulouridis, E., et al. 2018, *A&A*, 620, A5, doi: [10.1051/0004-6361/201731606](https://doi.org/10.1051/0004-6361/201731606)
- Aghanim, N., et al. 2016, *Astron. Astrophys.*, 596, A107, doi: [10.1051/0004-6361/201628890](https://doi.org/10.1051/0004-6361/201628890)
- Aguado-Barahona, A., Barrena, R., Streblyanska, A., et al. 2019, *Astron. Astrophys.*, 631, A148, doi: [10.1051/0004-6361/201936034](https://doi.org/10.1051/0004-6361/201936034)
- Alam, S., et al. 2017, *Mon. Not. Roy. Astron. Soc.*, 470, 2617, doi: [10.1093/mnras/stx721](https://doi.org/10.1093/mnras/stx721)

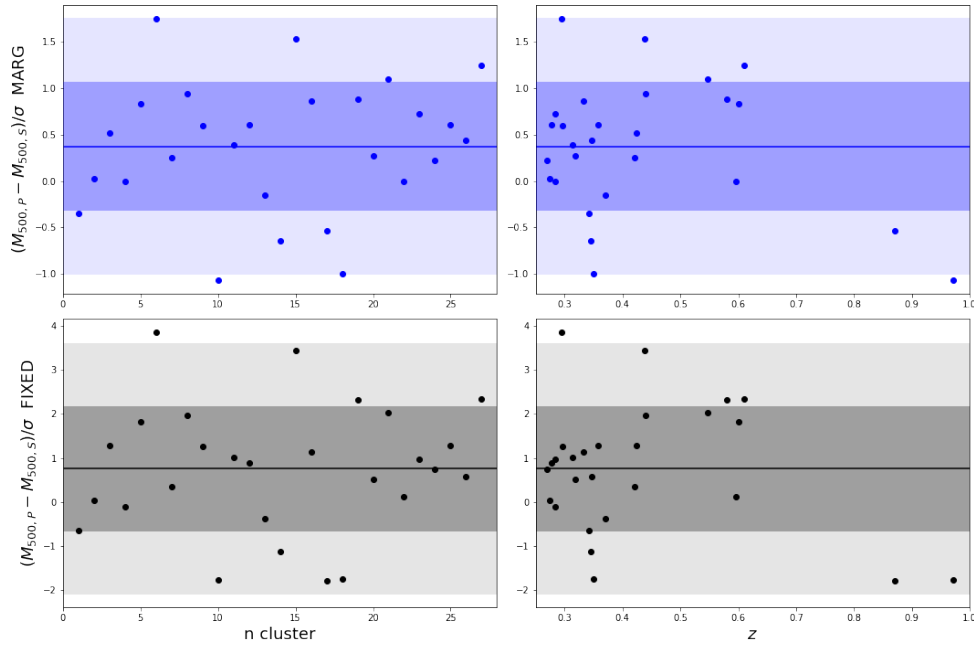


Figure 9. We show the distribution of mass differences for the 27 clusters in common between Planck and SPT-SZ cosmological catalogs, as a function of the cluster number (left) and redshift (right). We compare the results when considering the mass estimates marginalised over cosmological and scaling relation parameters (in blue, top panels) and obtained with fixed cosmological and scaling relation parameters (in black, bottom panels). The shaded areas represent the 1σ and 2σ intervals of the distribution.

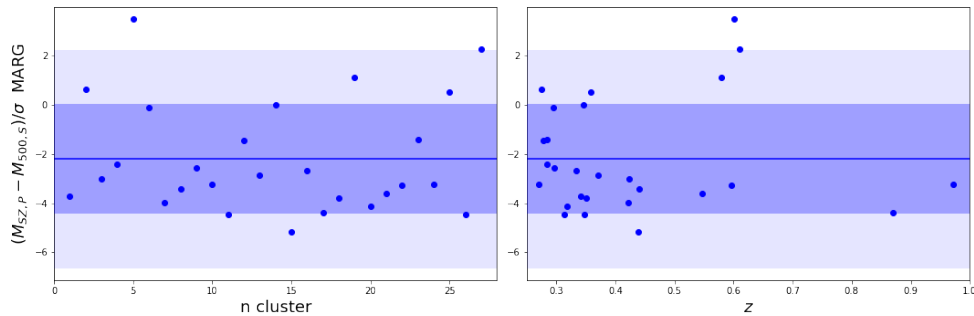


Figure 10. We show the distribution of mass differences for the 27 clusters in common between Planck and SPT-SZ cosmological catalogs, as a function of the cluster number (left) and redshift (right). For the Planck clusters, we consider M_{SZ} estimates. For the SPT-SZ clusters we consider the mass estimates marginalised over cosmological and scaling relation parameters. The shaded areas represent the 1σ and 2σ intervals of the distribution.

Allen, S. W., Evrard, A. E., & Mantz, A. B. 2011, *Ann.*

Rev. Astron. Astrophys., 49, 409,

doi: [10.1146/annurev-astro-081710-102514](https://doi.org/10.1146/annurev-astro-081710-102514)

Amodeo, S., et al. 2018, *Astrophys. J.*, 853, 36,

doi: [10.3847/1538-4357/aa98dd](https://doi.org/10.3847/1538-4357/aa98dd)

Arnaud, M., Pratt, G. W., Piffaretti, R., et al. 2010, *A&A*,

517, A92, doi: [10.1051/0004-6361/200913416](https://doi.org/10.1051/0004-6361/200913416)

Bertin, E., & Arnouts, S. 1996, *Astron. Astrophys. Suppl.*

Ser., 117, 393, doi: [10.1051/aas:1996164](https://doi.org/10.1051/aas:1996164)

Bertocco, S., Goz, D., Tornatore, L., et al. 2020, in

Astronomical Society of the Pacific Conference Series,

Vol. 527, *Astronomical Data Analysis Software and*

Systems XXIX, ed. R. Pizzo, E. R. Deul, J. D. Mol, J. de

Plaa, & H. Verkouter, 303.

<https://arxiv.org/abs/1912.05340>

Beutler, F., Blake, C., Colless, M., et al. 2011, *Monthly*

Notices of the Royal Astronomical Society, 416, 3017,

doi: [10.1111/j.1365-2966.2011.19250.x](https://doi.org/10.1111/j.1365-2966.2011.19250.x)

—, 2012, *Mon. Not. Roy. Astron. Soc.*, 423, 3430,

doi: [10.1111/j.1365-2966.2012.21136.x](https://doi.org/10.1111/j.1365-2966.2012.21136.x)

- Bleem, L., et al. 2015, *Astrophys. J. Suppl.*, 216, 27, doi: [10.1088/0067-0049/216/2/27](https://doi.org/10.1088/0067-0049/216/2/27)
- . 2020, *Astrophys. J. Suppl.*, 247, 25, doi: [10.3847/1538-4365/ab6993](https://doi.org/10.3847/1538-4365/ab6993)
- Boada, S., Hughes, J. P., Menanteau, F., et al. 2019, *Astrophys. J.*, 871, 188, doi: [10.3847/1538-4357/aaf3a0](https://doi.org/10.3847/1538-4357/aaf3a0)
- Bocquet, S., Heitmann, K., Habib, S., et al. 2020, *ApJ*, 901, 5, doi: [10.3847/1538-4357/abac5c](https://doi.org/10.3847/1538-4357/abac5c)
- Bocquet, S., et al. 2019, *Astrophys. J.*, 878, 55, doi: [10.3847/1538-4357/ab1f10](https://doi.org/10.3847/1538-4357/ab1f10)
- Böhringer, H., Chon, G., Retzlaff, J., et al. 2017, *Astron. J.*, 153, 220, doi: [10.3847/1538-3881/aa67ed](https://doi.org/10.3847/1538-3881/aa67ed)
- Carlstrom, J. E., et al. 2011, *Publ. Astron. Soc. Pac.*, 123, 568, doi: [10.1086/659879](https://doi.org/10.1086/659879)
- Cavaliere, A., & Fusco-Femiano, R. 1976, *Astron. Astrophys.*, 49, 137
- Chambers, K. C., Magnier, E. A., Metcalfe, N., et al. 2016, arXiv e-prints, arXiv:1612.05560. <https://arxiv.org/abs/1612.05560>
- de Haan, T., Benson, B. A., Bleem, L. E., et al. 2016, *ApJ*, 832, 95, doi: [10.3847/0004-637X/832/1/95](https://doi.org/10.3847/0004-637X/832/1/95)
- Dietrich, J., et al. 2019, *Mon. Not. Roy. Astron. Soc.*, 483, 2871, doi: [10.1093/mnras/sty3088](https://doi.org/10.1093/mnras/sty3088)
- Drlica-Wagner, A., et al. 2018, *Astrophys. J. Suppl.*, 235, 33, doi: [10.3847/1538-4365/aab4f5](https://doi.org/10.3847/1538-4365/aab4f5)
- Eckert, D., et al. 2019, *Astron. Astrophys.*, 621, A40, doi: [10.1051/0004-6361/201833324](https://doi.org/10.1051/0004-6361/201833324)
- Feroz, F., Hobson, M., & Bridges, M. 2009, *Mon. Not. Roy. Astron. Soc.*, 398, 1601, doi: [10.1111/j.1365-2966.2009.14548.x](https://doi.org/10.1111/j.1365-2966.2009.14548.x)
- Gianfagna, G., et al. 2021, *Mon. Not. Roy. Astron. Soc.*, 502, 5115, doi: [10.1093/mnras/stab308](https://doi.org/10.1093/mnras/stab308)
- Herbonnet, R., Sifon, C., Hoekstra, H., et al. 2020, *Mon. Not. Roy. Astron. Soc.*, 497, 4684, doi: [10.1093/mnras/staa2303](https://doi.org/10.1093/mnras/staa2303)
- Hilton, M., et al. 2021, *Astrophys. J. Suppl.*, 253, 3, doi: [10.3847/1538-4365/abd023](https://doi.org/10.3847/1538-4365/abd023)
- Hoekstra, H., Herbonnet, R., Muzzin, A., et al. 2015, *Mon. Not. Roy. Astron. Soc.*, 449, 685, doi: [10.1093/mnras/stv275](https://doi.org/10.1093/mnras/stv275)
- Huang, N., et al. 2020, *Astron. J.*, 159, 110, doi: [10.3847/1538-3881/ab6a96](https://doi.org/10.3847/1538-3881/ab6a96)
- Klein, M., Grandis, S., Mohr, J. J., et al. 2019, *MNRAS*, 488, 739, doi: [10.1093/mnras/stz1463](https://doi.org/10.1093/mnras/stz1463)
- Liu, A., et al. 2021. <https://arxiv.org/abs/2106.14518>
- Maturi, M., Bellagamba, F., Radovich, M., et al. 2019, *MNRAS*, 485, 498, doi: [10.1093/mnras/stz294](https://doi.org/10.1093/mnras/stz294)
- McClintock, T., Rozo, E., Becker, M. R., et al. 2019, *ApJ*, 872, 53, doi: [10.3847/1538-4357/aaf568](https://doi.org/10.3847/1538-4357/aaf568)
- McDonald, M., et al. 2013, *Astrophys. J.*, 774, 23, doi: [10.1088/0004-637X/774/1/23](https://doi.org/10.1088/0004-637X/774/1/23)
- . 2017, *Astrophys. J.*, 843, 28, doi: [10.3847/1538-4357/aa7740](https://doi.org/10.3847/1538-4357/aa7740)
- Melin, J.-B., & Bartlett, J. G. 2015, *Astron. Astrophys.*, 578, A21, doi: [10.1051/0004-6361/201424720](https://doi.org/10.1051/0004-6361/201424720)
- Melin, J.-B., Bartlett, J. G., & Delabrouille, J. 2006, *Astron. Astrophys.*, 459, 341, doi: [10.1051/0004-6361:20065034](https://doi.org/10.1051/0004-6361:20065034)
- Melin, J. B., Bartlett, J. G., Tarrío, P., & Pratt, G. W. 2021, *Astron. Astrophys.*, 647, A106, doi: [10.1051/0004-6361/202039471](https://doi.org/10.1051/0004-6361/202039471)
- Monaco, P. 2016, *Galaxies*, 4, 53, doi: [10.3390/galaxies4040053](https://doi.org/10.3390/galaxies4040053)
- Okabe, N., & Smith, G. P. 2016, *Mon. Not. Roy. Astron. Soc.*, 461, 3794, doi: [10.1093/mnras/stw1539](https://doi.org/10.1093/mnras/stw1539)
- Pacaud, F., Pierre, M., Melin, J. B., et al. 2018, *A&A*, 620, A10, doi: [10.1051/0004-6361/201834022](https://doi.org/10.1051/0004-6361/201834022)
- Penna-Lima, M., Bartlett, J. G., Rozo, E., et al. 2017, *Astron. Astrophys.*, 604, A89, doi: [10.1051/0004-6361/201629971](https://doi.org/10.1051/0004-6361/201629971)
- Planck Collaboration, Ade, P. A. R., Aghanim, N., et al. 2014, *A&A*, 571, A20, doi: [10.1051/0004-6361/201321521](https://doi.org/10.1051/0004-6361/201321521)
- . 2016a, *A&A*, 594, A27, doi: [10.1051/0004-6361/201525823](https://doi.org/10.1051/0004-6361/201525823)
- . 2016b, *A&A*, 594, A24, doi: [10.1051/0004-6361/201525833](https://doi.org/10.1051/0004-6361/201525833)
- Planck Collaboration, Aghanim, N., Akrami, Y., et al. 2020a, *A&A*, 641, A6, doi: [10.1051/0004-6361/201833910](https://doi.org/10.1051/0004-6361/201833910)
- . 2020b, *A&A*, 641, A1, doi: [10.1051/0004-6361/201833880](https://doi.org/10.1051/0004-6361/201833880)
- . 2020c, *A&A*, 641, A3, doi: [10.1051/0004-6361/201832909](https://doi.org/10.1051/0004-6361/201832909)
- Pratt, G. W., Arnaud, M., Biviano, A., et al. 2019, *Space Sci. Rev.*, 215, 25, doi: [10.1007/s11214-019-0591-0](https://doi.org/10.1007/s11214-019-0591-0)
- Ross, A. J., Samushia, L., Howlett, C., et al. 2015, *Mon. Not. Roy. Astron. Soc.*, 449, 835, doi: [10.1093/mnras/stv154](https://doi.org/10.1093/mnras/stv154)
- Salvati, L., Douspis, M., & Aghanim, N. 2018, *Astron. Astrophys.*, 614, A13, doi: [10.1051/0004-6361/201731990](https://doi.org/10.1051/0004-6361/201731990)
- Salvati, L., Douspis, M., Ritz, A., Aghanim, N., & Babul, A. 2019, *Astron. Astrophys.*, 626, A27, doi: [10.1051/0004-6361/201935041](https://doi.org/10.1051/0004-6361/201935041)
- Schrabback, T., et al. 2018, *Mon. Not. Roy. Astron. Soc.*, 474, 2635, doi: [10.1093/mnras/stx2666](https://doi.org/10.1093/mnras/stx2666)
- Sereno, M., Covone, G., Izzo, L., et al. 2017, *Mon. Not. Roy. Astron. Soc.*, 472, 1946, doi: [10.1093/mnras/stx2085](https://doi.org/10.1093/mnras/stx2085)
- Sereno, M., & Ettori, S. 2015, *Mon. Not. Roy. Astron. Soc.*, 450, 3675, doi: [10.1093/mnras/stv814](https://doi.org/10.1093/mnras/stv814)

- Smith, G. P., et al. 2016, *Mon. Not. Roy. Astron. Soc.*, 456, L74, doi: [10.1093/mnrasl/slv175](https://doi.org/10.1093/mnrasl/slv175)
- Sunyaev, R. A., & Zeldovich, Y. B. 1970, *Astrophys. Space Sci.*, 7, 20
- Taffoni, G., Becciani, U., Garilli, B., et al. 2020, in *Astronomical Society of the Pacific Conference Series*, Vol. 527, *Astronomical Data Analysis Software and Systems XXIX*, ed. R. Pizzo, E. R. Deul, J. D. Mol, J. de Plaa, & H. Verkouter, 307.
<https://arxiv.org/abs/2002.01283>
- Tinker, J. L., Kravtsov, A. V., Klypin, A., et al. 2008, *Astrophys. J.*, 688, 709, doi: [10.1086/591439](https://doi.org/10.1086/591439)
- von der Linden, A., et al. 2014, *Mon. Not. Roy. Astron. Soc.*, 443, 1973, doi: [10.1093/mnras/stu1423](https://doi.org/10.1093/mnras/stu1423)
- Zubeldia, I. n., & Challinor, A. 2019, *Mon. Not. Roy. Astron. Soc.*, 489, 401, doi: [10.1093/mnras/stz2153](https://doi.org/10.1093/mnras/stz2153)
- Zuntz, J., Paterno, M., Jennings, E., et al. 2015, *Astron. Comput.*, 12, 45, doi: [10.1016/j.ascom.2015.05.005](https://doi.org/10.1016/j.ascom.2015.05.005)